Laser-Induced Periodic Surface Structures—A Scientific Evergreen

Jörn Bonse, Sandra Höhm, Sabrina V. Kirner, Arkadi Rosenfeld, and Jörg Krüger

(Invited Paper)

***Abstract*—Laser-induced periodic surface structures (LIPSS, ripples) are a universal phenomenon and can be generated on almost any material upon irradiation with linearly polarized radiation. With the availability of ultrashort laser pulses, LIPSS have gained an increasing attraction during the past decade, since these structures can be generated in a simple single-step process, which allows a surface nanostructuring for tailoring optical, mechanical, and chemical surface properties. In this study, the current state in the field of LIPSS is reviewed. Their formation mechanisms are analyzed in ultrafast time-resolved scattering, diffraction, and polarization constrained double-pulse experiments. These experiments allow us to address the question whether the LIPSS are seeded via ultrafast energy deposition mechanisms acting during the absorption of optical radiation or via self-organization after the irradiation process. Relevant control parameters of LIPSS are identified, and technological applications featuring surface functionalization in the fields of optics, fluidics, medicine, and tribology are discussed.**

***Index Terms*—Laser ablation, laser applications, materials processing, nanostructures, optical polarization, periodic structures, plasmons, self-assembly, surface texture, ultrafast optics.**

I. Introduction

LASER-induced periodic surface structures (LIPSS), often termed *ripples*, are a universal phenomenon that occurs on solids upon irradiation with linearly polarized laser radiation [1]. LIPSS usually emerge as a surface relief composed of (quasi-) periodic lines, which exhibit a clear correlation to the wavelength and polarization of the radiation. These structures can be generated on almost any material (metals, semiconductors, and dielectrics) [2] and are formed in a huge range of pulse durations, ranging from continuous wave irradiation [3] down to only a few femtoseconds (fs) [4].

Manuscript received July 29, 2016; revised September 16, 2016; accepted September 20, 2016. Date of publication October 3, 2016; date of current version December 6, 2016. This work was supported in part by the German Science Foundation under Grants KR 3638/1-2 and RO 2074/7-2, and in part by the European Horizon 2020—FETOPEN Project "LiNaBioFluid" under Grant 665337.

J. Bonse, S. V. Kirner, and J. Krüger are with the Bundesanstalt für Materialforschung und –prüfung, Berlin 12205, Germany (e-mail: joern.bonse@bam.de; sabrina.kirner@bam.de; joerg.krueger@bam.de).

S. Höhm and A. Rosenfeld are with the Max-Born-Institut für Nichtlineare Optik und Kurzzeitspektroskopie, Berlin 12489, Germany (e-mail: hoehm@mbi-berlin.de; rosenfeld@mbi-berlin.de).

Color versions of one or more of the figures in this paper are available online at http://ieeexplore.ieee.org.

Digital Object Identifier 10.1109/JSTQE.2016.2614183

From a fundamental point of view, LIPSS are challenging as their formation involves a complex sequence of inter- and intrapulse physical processes. Absorption of radiation by the electronic system of the irradiated material is followed by the transfer of the deposited energy to the lattice system of the solid and by a variety of subsequent thermal and possibly hydrodynamical or chemical effects. Those events may affect the formation of the final periodic surface relief in most cases via spatially modulated material removal (ablation). Due to the variety of mechanisms and the importance of additional "feedback phenomena" as a consequence of repetitive (multiple-pulse) surface irradiation, a comprehensive theory of LIPSS is currently not available and several aspects are still controversially discussed in literature.

From the technological point of view, the processing of LIPSS represents an impressively simple approach, which can be used for various applications. The nanostructures can be generated in a single-step process that enables surface functionalization toward a control of optical, mechanical, or chemical surface properties. The manufacturing process can be implemented either serially or parallel (in-line). It is executable in air environment and, thus, avoids cost-expensive and time-consuming vacuum technologies or additional chemical procedures.

This article continues a series of reviews on LIPSS [5]–[10]. While the state-of-the-art up to the middle of the eighties of the past century was comprehensively summarized by Siegman and Fauchet [6] and Akhmanov *et al.* [5], some recent contributions focused on the significantly increasing research activities performed in the field of LIPSS during the past decade [7]–[10]. This emerging research is demonstrated in Fig. 1, which provides the number of publications per year during the last four decades (analyzed by specific search terms entered to the *ISI Web of Knowledge database*). Currently, approximately 80 publications annually appear in the scientific literature and most of them are related to the use of femtosecond laser pulses. The present work complements and extends our previous review article [2] published in 2012.

II. Historical Developments

A. The Early Years

Since the discovery of LIPSS by Birnbaum in 1965 [11], their investigation has developed into a scientific evergreen. Birnbaum reported the formation of LIPSS on polished germanium

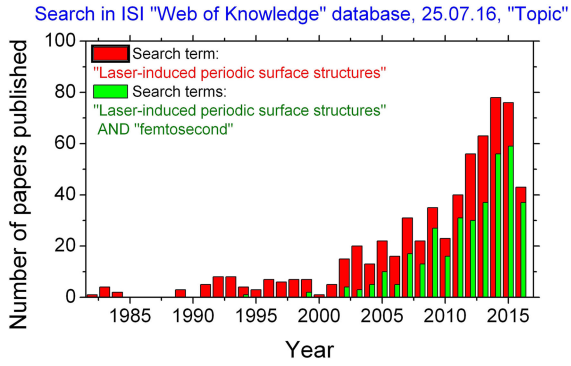

Fig. 1. Research activities in the field of LIPSS, exemplified by the number of papers published per year - matching on July 25th 2016 in the *ISI Web of Knowledge database* to the search term "Laser-induced periodic surface structures" or the two logically connected terms "Laser-induced periodic surface structures" AND "Femtosecond".

single-crystal surfaces after irradiation by a focused ruby laser beam. He attributed their formation to a diffraction effect and suggested that the surface relief is formed by material removal at the maxima of the electric field intensity [11]. A few years later, in 1973, Emmony *et al.* suggested that LIPSS are generated via interference of the incident laser beam with light scattered at surface defects and scratches [12]. For pulsed laser systems, it turned out very early that, apart from the irradiation wavelength λ and polarization direction, the laser fluence (peak value ϕ_0) and the number of pulses applied to the irradiated spot (N) are the key to control the occurrence of LIPSS experimentally.

B. The 1980's

At the beginning of the 1980s, Keilmann and Bai extended the idea of Emmony *et al.* by proposing that LIPSS are originating from an interference of the incident radiation with surface polaritons bound to and propagating along the irradiated surface [13]. Almost at the same time, two research groups around Sipe and Siegman independently proposed extended theories for the formation of LIPSS [14], [15]. Sipe and co-workers developed a first-principles theory of LIPSS and launched this terminology (*laser-induced periodic surface structures*, LIPSS) in 1982 to the literature (see Fig. 1) [1]. In a following series of three pioneering publications [14], [16], [17] these authors theoretically and experimentally analyzed the interactions of electromagnetic radiation with a microscopically rough surface by introducing the so-called *efficacy factor* η. The latter represents a scalar function which is proportional to the inhomogeneous energy deposition into the irradiated material [14]. η describes the efficacy with which the surface roughness leads to inhomogeneous absorption of radiation and predicts possible LIPSS wave vectors $\boldsymbol{k}$ of the surface [with $|\boldsymbol{k}| = (2\pi)/\Lambda$] as a function of the laser parameters (wavelength λ, angle of incidence θ, polarization direction, and wave vector of the incident radiation) and surface parameters (dielectric permittivity ε and surface roughness). A simplified set of complex-valued equations was derived more than twenty years later, which allows a straightforward calculation of η [18].

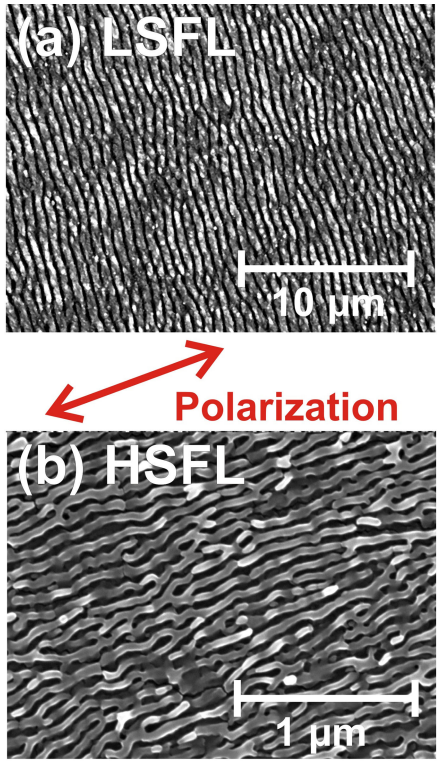

Fig. 2. Scanning electron micrographs of two different types of LIPSS formed on titanium alloy (Ti6Al4V) surfaces after irradiation with fs-laser pulses [30 fs, 800 nm, 1 kHz]. (a) LSFL [$\phi_0 = 0.11\,\mathrm{J/cm^2}$, $N \sim 56$]; (b) HSFL [$\phi_0 = 0.08\,\mathrm{J/cm^2}$, $N \sim 560$]. Note the different magnifications.

The efficacy factor theory is the currently most widely accepted theory of LIPSS and explicitly includes *surface-scattered electromagnetic waves* (SEW). However, it has to be noted that this theory does not include any feedback phenomena and that some types of LIPSS are not properly described by it [18]–[20].

C. The New Millennium

At the turn of the new millennium, the number of annual publications in the field of LIPSS started to grow significantly, see the red bar charts in Fig. 1 which are associated with the search term <laser-induced periodic surface structures>. This still ongoing trend is caused by the observation of a "non-classical" type of LIPSS with periods significantly smaller than the irradiation wavelength [21]–[25]. These structures are termed *high spatial frequency LIPSS* (HSFL), or sometimes *nanoripples*, and must clearly be distinguished from the classical near-wavelength sized LIPSS, called *low spatial frequency LIPSS* (LSFL). It was suggested by Reif and co-workers that the HSFL are formed via a self-reorganization of the irradiated material, associated with a surface instability as a result of surface erosion and atomic diffusion effects [26].

Fig. 2 exemplifies both types of nanostructures via scanning electron micrographs (SEM) of LSFL [see Fig. 2(a)] and HSFL [see Fig. 2(b)] formed on a polished titanium alloy (Ti6Al4V) surface after irradiation with multiple Ti:sapphire fs-laser pulses (30 fs, 800 nm, 1 kHz). For the given conditions, the LSFL on Ti6Al4V have periods $\Lambda_{\mathrm{LSFL}} \sim (620 \pm 80)$ nm and are formed

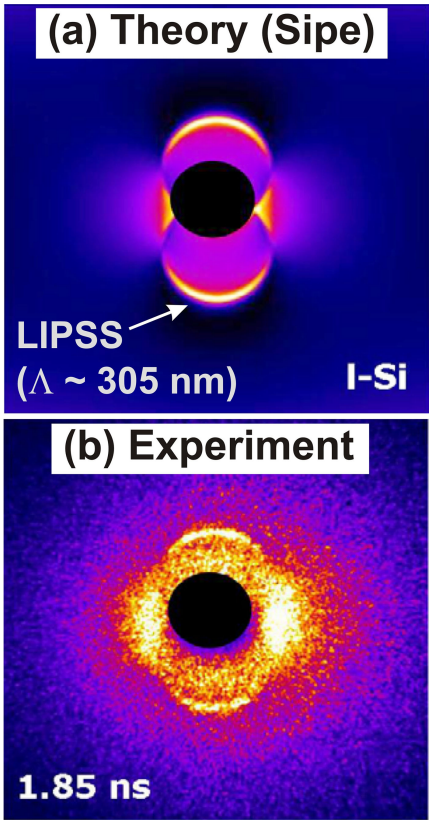

Fig. 3. Comparison of the calculated efficacy factor η assuming LIPSS on liquid silicon (a) and the experimentally scattered XUV-radiation (b) [$\lambda_{\mathrm{Probe}} = 13.5\,\mathrm{nm}$, $\tau_{\mathrm{Probe}} = 30\,\mathrm{fs}$, $\theta_{\mathrm{Probe}} = 0°$] measured at a delay of $\Delta t = 1.85\,\mathrm{ns}$ after exciting a rough 100 nm thick silicon film by a single ps-laser pulse [$\lambda_{\mathrm{Pump}} = 527\,\mathrm{nm}$, $\tau_{\mathrm{Pump}} = 12\,\mathrm{ps}$, $\theta_{\mathrm{Pump}} = 45°$]. The black disks represent the beam block of the zero-order signal. Figure adapted from [29].

perpendicular to the laser beam polarization, while the HSFL exhibit periods of $\Lambda_{\mathrm{HSFL}} \sim (80 \pm 20)\,\mathrm{nm}$ only and are oriented parallel to the polarization. These LIPSS periods were determined by two-dimensional spatial Fourier transforms, which allows the evaluation of entire images. The corresponding surface modulation depths of the LIPSS were measured by scanning force microscopy and account to (110 ± 20) nm for the LSFL and (25 ± 10) nm for the HSFL.

In 2009, the theory of Sipe was combined with a Drude model for considering the optical response of the quasi-free conduction band electrons of the laser excited solids [27], [28]. This approach successfully describes LIPSS in zinc oxide and silicon and confirmed the importance of transient changes of the dielectric permittivity during the early stage of LIPSS formation on semiconductors upon irradiation with ultrashort laser pulses.

In 2010, a group of researchers around Sokolowski-Tinten provided a direct experimental proof of Sipes theory by studying the dynamics of the formation of LIPSS on rough silicon films in time-resolved ps-optical pump/fs-XUV scattering experiments [29]. Almost quantitative agreement between the spatially scattered XUV-radiation pattern and the efficacy factor was found, see Fig. 3.

Two years later, Skolski *et al.* numerically studied the formation of LIPSS by employing finite-difference time-domain calculations (FDTD) to solve the Maxwell-equations at a statistically rough surface [30]. This approach allowed to qualify the inhomogeneous absorption in laser-excited silicon and confirmed the validity of the analytical Sipe-Drude model in the near surface region. The FDTD-approach was extended also to larger sample depths, which are not directly accessible in Sipes theory [30]–[32]. In an alternative approach, FDTD was used to calculate the optical absorption in idealized nanostructures and surface gratings, allowing to visualize plasmonic dispersion relations, optical nearfields in the surface nanostructures, and to identify feedback mechanisms [33]–[35].

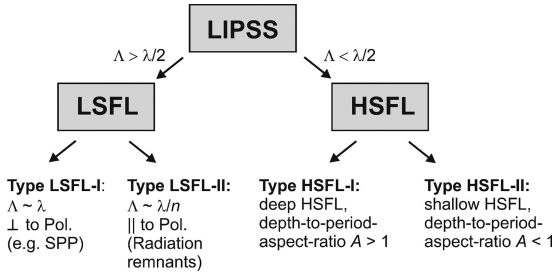

Fig. 4. Classification scheme of fs-laser-induced periodic surface structures.

III. Mechanisms of LIPSS formation

For normal incident radiation LSFL typically exhibit periods close to or slightly smaller than the irradiation wavelength $(\lambda/2 \leq \Lambda_{\mathrm{LSFL}} \leq \lambda)$, while HSFL have periods smaller than half of the irradiation wavelength $(\Lambda_{\mathrm{HSFL}} < \lambda/2)$. HSFL are observed predominantly for laser pulse durations in the fs- to ps-range. Hence, the ever-growing availability of ultrafast laser systems strongly promotes the current research on LIPSS. The latter argument is directly supported by the data provided as green bars added in Fig. 1, which indicate that in the new millennium the majority of publications on LIPSS are based on fs-laser sources. Both types of LIPSS (LSFL and HSFL) can be divided into two sub-categories (see Fig. 4).

A. LSFL

On strong absorbing materials, such as semiconductors and metals, the LSFL are usually oriented perpendicular to the laser beam polarization and exhibit periods close to the wavelength, i.e., deviating not more than a few tens of percent $(\Lambda_{\mathrm{LSFL}} \sim \lambda)$. This type of LIPSS is called *LSFL-I* in the following and is exemplified in Fig. 2(a). It is generally accepted that these structures are generated by interaction of the incident laser beam with an electromagnetic wave scattered at the rough surface and may involve the excitation of *Surface Plasmon Polaritons* (SPP) [14], [28], [29], [33], [36], [37]. Particularly for irradiation with ultrashort laser pulses this excitation channel is of major importance since initially plasmonically non-active materials (dielectrics and semiconductors) can transiently be turned into a metallic state, which allows a direct excitation of SPP [$\mathrm{Re}(\varepsilon) < -1$], once a critical density of electrons in the conduction band is exceeded [28], [33], [38], [39].

For simplicity, in the LIPSS literature often the SPP wavelength is directly linked to the *LSFL-I* periodicity $(\Lambda_{\mathrm{LSFL}} = \Lambda_{\mathrm{SPP}})$. In the "standard surface plasmon polariton model" of a

plane metal-air interface for normal incident radiation, the SPP spatial period Λ_{SPP} is related to the bulk dielectric permittivity ε via $\Lambda_{\mathrm{LSFL}} = \Lambda_{\mathrm{SPP}} = \lambda \times \mathrm{Re}\{[(\varepsilon+1)/\varepsilon]^{1/2}\}$ [37], [40], [41]. For a small number of laser pulses, the LSFL period may coincide with Λ_{SPP} as the surface corrugations are still small (depths $d << \lambda$). However, it should be underlined that once a sufficiently deep surface relief has formed, the simple expression of Λ_{SPP} is not valid anymore [42]. Also multi-pulse feedback phenomena significantly affect the LSFL formation (see Section III-C below). Hence, the applicability of the simple "standard surface plasmon polariton model" always has to be checked carefully.

On dielectrics and when the single photon energy is smaller than the band gap energy of the materials, another type of LSFL is observed. These *LSFL-II* structures are typically oriented parallel to the laser beam polarization and have spatial periods close to $\Lambda_{\mathrm{LSFL}} = \lambda/n$, with $n = \varepsilon^{1/2}$ being the refractive index of the dielectric material [14], [43]–[45]. These structures are related to so-called *Radiation Remnants* (RR), which were predicted already by the LIPSS theory of Sipe *et al.* for transparent materials [14]. The RR represent a specific non-propagating electromagnetic mode close to the rough surface [46], which is capable of extracting energy from the incident radiation and transferring it to the material at the associated spatial frequencies.

Under specific irradiation conditions, i.e., in a certain fluence range, near field enhancement or grating assisted effects can lead to a splitting of the LSFL ridges already formed at the surface [34], [47]. As a result, the LSFL discontinuously transform into another LIPSS structure with only half of the spatial period. As this formation mechanism is directly linked to the LSFL morphologies, these LIPSS are not distinguished as distinct type of LIPSS here.

The relevance of the local polarization state on the LSFL formation was recently demonstrated by Nivas *et al.*, who generated optical vortex beams with locally varying polarization by means of spatial light modulators [48]. They demonstrated that for radial, azimuthal, or spiral-like polarized fs-laser beams the LSFL strictly follow the orientation of the local (linear) polarization direction (being perpendicular to it).

Finally, it should be noted that *LSFL-I* can form also in the non-ablative regime via local melting and rapid solidification phenomena. The origin also lies in the excitation of a SEW, but the deposited optical energy is not sufficient for material removal. However, the rapid solidification of the molten regions can lead to local changes of the near-surface material structure, resulting in a periodic pattern of amorphous and crystalline regions [49], [50]. Additionally, thermocapillary and chemicapillary forces may act on the locally molten material leading to a spatial redistribution of material during the melt duration [51], [52]. Some authors have even reported the formation of LIPSS at fluences below the melting threshold of the irradiated material, where surface diffusion effects, defect-driven instabilities, or thermoplastic deformations may corrugate the surface [53]–[55].

LIPSS formed under such sub-ablation or sub-melting conditions can even protrude above the original surface [54], [56], [57]. However, both sub-ablative LIPSS formation mechanisms require a sufficient dosage of surface mobility provided to the material and, thus, have a tendency to form at large numbers of laser pulses (typically exceeding several thousands) or for long pulse durations.

B. HSFL

HSFL with periods smaller than half of the wavelength are formed at fluences very close to the damage threshold of the irradiated material and predominantly for pulse durations in the fs- to ps-range. HSFL are oriented either parallel or perpendicular to the laser beam polarization, depending on the material (see the table in [2]). They manifest in two different forms (compare Fig. 4). Type *HSFL-I* is mainly observed on dielectrics and semiconductors and consist of very narrow periodic grooves having widths *w* of a few tens of nanometer only $(w \ll \Lambda_{\mathrm{HSFL}})$. The *HSFL-I* formation may initially start from individual nanocracks and their groove depth *d* can reach up to several hundreds of nanometers $(d > \Lambda_{\mathrm{HSFL}})$ [58]–[60], resulting in a depth-to-period aspect ratio $A = d/\Lambda_{\mathrm{HSFL}} > 1$. Therefore, some authors call these nanostructures *deep-subwavelength ripples* [33], [34]. For (semi)transparent materials *HSFL-I* often exhibit periods of $\Lambda_{\mathrm{HSFL}} \sim \lambda/(2n)$ [9].

In contrast, the grooves of the second type *HSFL-II* exhibit depths of only a few tens of nanometers along with periods approaching the sub-100 nm range, resulting in a depth-to-period aspect ratio $A << 1$. These shallow HSFL are often observed on metal surfaces, such as titanium [19], [61] or nickel [62] and it was suggested that superficial oxidation [19], [63] or twinning effects during the resolidification of a shallow laser-induced melt layer [62] are involved in their formation.

However, currently these two HSFL types are not distinguished in scientific literature and the origin of HSFL is controversially discussed. Apart from the already mentioned mechanisms of self-organization, oxidation and twinning, also second harmonic generation [25], [27], evanescent fields at nanocorrugated dielectric surfaces [64] and the involvement of different plasmonic effects [65]–[67] were proposed.

From the three experimental observations that HSFL (i) mainly form upon irradiation with ultrashort laser pulses, (ii) are strictly related to the direction of the linear laser polarization, and (iii) have a lower period limit around 50 to 100 nm puts a preference on ultrafast energy deposition mechanisms to the sample surface as origin of the HSFL. The lower period limit is caused by thermal diffusion effects washing out too small spatial modulations during the transfer of the energy from the optically excited electronic system to the lattice of the solid. Regarding a theoretical description of the absorbed optical energy, it should be noted that the HSFL are not properly described by Sipes theory [18], [19]. Hence, numerical methods are recommended here [30]–[32].

C. Feedback in LIPSS Formation

Although optical interference and scattering effects can be imprinted into the surface topography already by a single laser pulse [28], [35], pronounced and well-aligned LIPSS are usually

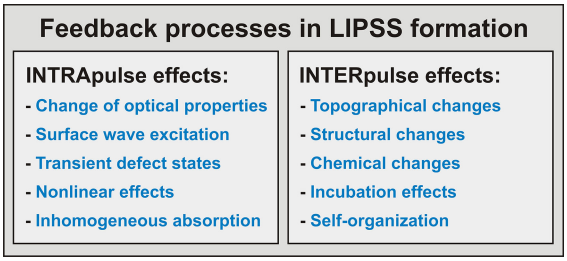

Fig. 5. Feedback processes in LIPSS formation.

formed after irradiation by multiple laser pulses. The first pulse generates a rough surface which facilitates the coupling of energy for the following laser pulses. Specific spatial frequencies of the roughness distribution can better absorb radiation. During repetitive exposure, via this *positive feedback*, certain spatial periods are favored to form the grating like LIPSS pattern.

Fig. 5 compiles feedback processes in LIPSS formation, which can occur already during a single laser pulse (*intrapulse effects*) or which may occur between successive pulses (*interpulse effects*).

Intrapulse effects can include transient changes of the optical properties of the solid [15], [68], [69], the stimulation of SEW [5], [14], [70], the excitation of transient defect states (such as self-trapped excitons [71]), nonlinear effects (e.g. second harmonic generation) [25], [27] or spatially inhomogeneous absorption [72].

The excitation of SEW and the corresponding directional scattering and field enhancement characteristics [73] during the laser pulse have important consequences for the processing of LIPSS. It was already observed in 1982 by Fauchet and Siegman that, upon line scanning of focused ps-laser pulses across a germanium wafer surface, the LIPSS can be "coherently linked" when the laser irradiation spots have a spatial overlap [74]. Recently, Ruiz de la Cruz *et al.* demonstrated that the *LSFL-I* regularity on chromium films can be significantly improved if the scanning direction of the laser beam is perpendicular to its linear polarization [75].

Interpulse effects influence the surface morphologies via ablation [31] or hydrodynamical melt flows [17], [57], [76], alterations of the material structure at the surface between crystalline or amorphous states [18], [77]–[79], which affect the optical constants. Additionally, chemical reactions with the ambient environment, such as oxidation [21], [80], [81], incubation effects generating permanent defect states [53], [54] reducing the damage thresholds, or self-organization promoting surface erosion and diffusion of atoms are feasible [26].

An interpulse feedback mechanism relevant for ultrafast laser processing of LSFL was proposed by Huang *et al.,* who analyzed the resonant coupling of SPP to the periodic surface structures [33]. According to the authors the decrease in the LSFL period for an increasing number of laser pulses occurs via a grating-assisted surface plasmon-laser coupling: when the grating-like LSFL surface relief formed during the first few laser pulses deepens, the resonant wavelength of the SPP undergoes a shift, which leads to a decrease in the LSFL periods.

IV. Control and Dynamics of LIPSS

A. Single-Pulse Sequences

As discussed in the previous sections, the most direct way for experimentally manipulating LIPSS is based on irradiation by multiple single-pulse sequences. The appearance of LIPSS can be controlled by the irradiation wavelength λ, the angle of incidence θ, the polarization state, the laser peak fluence ϕ_0, the number of pulses N applied to the irradiated spot, and the refractive index n_0 of the ambient medium.

It is generally known that the LSFL period scales linearly with the irradiation wavelength $\Lambda_{\mathrm{LSFL}} = C \times \lambda$, although the slope C depends on the specific material parameters and irradiation conditions, see for example [82]–[84]. The dependence of the LIPSS periods on the angle of incidence has already been studied in detail by [5], [6], [14], [15], [70], [85]. Depending on the polarization direction (s- or p-polarized) and the angle of incidence, the LSFL period was predicted to follow the relation $\Lambda_{\mathrm{LSFL,p}} \sim \lambda/[\xi \pm \sin\theta]$, and $\Lambda_{\mathrm{LSFL,s}} \sim \lambda/[\xi^2 - \sin^2\theta]^{1/2}$, with $\xi^2 = |\mathrm{Re}(\varepsilon)|/[|\mathrm{Re}(\varepsilon)| - 1]$ [5]. For strong absorbing and plasmonic materials [$\mathrm{Re}(\varepsilon) << -1$] these equations simplify to the relations $\Lambda_{\mathrm{LSFL,p}} \sim \lambda/[1 \pm \sin\theta]$ and $\Lambda_{\mathrm{LSFL,s}} \sim \lambda/\cos\theta$, as theoretically predicted in the efficacy factor theory [14].

The local fluence has a tremendous impact on LIPSS. As already seen in Fig. 2, depending on the fluence, different types of LIPSS (LSFL and HSFL) appear on the same material. Moreover, for dielectrics, a transition between the *Radiation Remnant*-based LSFL (type II) and the plasmonic LSFL (type I) can be induced with increasing fluence. This occurs when enough laser-induced carriers are generated in the conduction band to promote plasmonic activity [43]. Within a specific type of LIPSS, several authors already studied the impact of the fluence on the spatial periods. For most materials, a moderate increase of Λ_{LSFL} with fluence is observed [19], [38], [43], [86], [87].

Another parameter to control the LIPSS period is the number of pulses N applied to the irradiated spot. For metals and semiconductors, an increase of N typically results in a decrease of Λ_{LSFL} by several tens of percent [19], [33], [88]. The origin lies in a multitude of intra- and interpulse feedback mechanisms, as already discussed in the previous Section III-C.

Apart from irradiation parameters, the ambient medium can significantly reduce the LIPSS periods. Particularly, for irradiation with ultrashort laser pulses in liquids, Λ_{LSFL} was reduced down to $0.1 \times \lambda - 0.4 \times \lambda$, while keeping the LIPSS orientation [80], [89]–[91].

B. Double-Pulse Sequences

While for continuous wave or pulsed laser processing with durations down to the ns-range the absorption of radiation and the laser-induced material removal temporally overlap, the availability of ultrashort laser pulses with durations in the fs- to ps-range allows to directly address the controversial question if the origin of LIPSS lies in the early stage of energy deposition to the material (*hypothesis I*), or in the subsequent self-organized

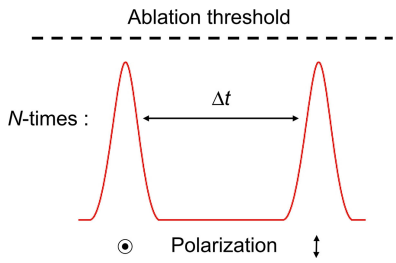

Fig. 6. Scheme of a sub-threshold double-fs-pulse sequence. For a detailed explanation of the corresponding experimental setup refer to [92].

reorganization of material (*hypothesis II*). That question can be explored in two complementary approaches, by (i) tailoring the optical energy deposition process by temporal beam shaping (e.g. in double-fs-pulse experiments) or by (ii) studying the ultrafast dynamics of LIPSS in time-resolved (pump-probe) experiments (see Section IV-C).

Evidence for *hypothesis I* is provided by the first approach, i.e., double-fs-pulse experiments, as realized in a Mach–Zehnder interferometric setup [92]. Multiple sequences of 800-nm double-pulses (N_{DPS}) were directly focused to the surface of different materials (fused silica, silicon, titanium). Each sequence (see Fig. 6) consists of two individual cross-polarized 50-fs pulses separated by a delay Δt. The peak fluence of each pulse was chosen below the respective (multipulse) damage threshold, i.e., only the joint action of both pulses led to LIPSS formation (sub-threshold condition). In the following $\phi_{0,\mathrm{tot}}$ represents the total fluence accumulated over both pulses of a sequence.

Results of equal energy double-fs-pulse irradiation are visualized in Fig. 7. It presents a collage of scanning electron micrographs of the three different material classes after double-pulse irradiation [fused silica (a)–(c), silicon (d)—(f) and titanium (g)—(i)] for delays Δt between 53 ps and +70 ps. The orientation of the laser beam polarization of the first pulse arriving to the sample surface is indicated by red arrows in Fig. 7(a) and (c).

On the dielectric fused silica at a short negative delay ($\Delta t = -0.1$ ps) vertically oriented *LSFL-II* can be seen parallel to the polarization of the first laser pulse [see Fig. 7(a)]. From experiments with multiple single-pulse sequences it is known that LSFL on that material form parallel to the polarization [43]. Hence, the first pulse of the double-pulse sequence determines the LIPSS orientation. For delay variations of less than 200 fs from negative to positive delays, the *LSFL-II* pattern is rotated by 90° [see Fig. 7(c)] along with the polarization of the first pulse. At zero-delay, when both pulses are temporally coinciding, the LSFL pattern appears at an angle of 45° between both polarization directions, i.e., parallel to their vectorial superposition [see Fig. 7(b)]. Here, the rippled surface area is increased since more electrons can be excited through nonlinear absorption for temporally overlapping pulses [93]

As shown in a series of previous publications [43], [92]–[94], for fused silica the first pulse of each double-pulse sequence always determines the spatial characteristics (period, orientation) of the *LSFL-II*. This pulse generates a spatially modulated carrier distribution in the conduction band via intrapulse electromagnetic scattering at the surface and nonlinear multi-photon absorption. These carriers then start to form self-trapped excitons (STE) as precursors of permanent color centers. The STE already carry the geometrical characteristics of the LSFL. The laser-induced carrier distribution is further amplified by the second fs-laser-pulse until the damage threshold of the surface is locally exceeded. This effect is reinforced by repetitive irradiation ($N_{\mathrm{DPS}} = 5$) due to incubation effects, finally leading via ablation to a surface relief in the form of LSFL with characteristics seeded by the first pulse.

On the semiconductor silicon at a negative delay of $\Delta t = -0.9$ ps *LSFL-I* perpendicular to the polarization of the second laser pulse arise [see Fig. 7(d)]. Experiments utilizing single-pulse sequences revealed that LSFL on silicon form perpendicular to the polarization [4]. For a positive delay of $\Delta t = +1.1$ ps, the *LSFL-I* pattern is again rotated by 90° [see Fig. 7(f)]. Opposed to the previous case of fused silica, on silicon the second pulse of the double-pulse sequence determines the LIPSS orientation. Similar to fused silica at zero-delay the LSFL pattern forms at an angle of 45° between both polarization directions [see Fig. 7(e)].

Previous publications have already shown that for silicon the second pulse of each double-pulse sequence determines the *LSFL-I* characteristics (period, orientation) [92], [93], [95]. The first pulse generates via one- and two-photon absorption carriers in the conduction band (CB) of the silicon without turning the semiconductor plasmonically active [$\mathrm{Re}(\varepsilon) > -1$]. The second laser pulse generates additional carriers in the CB, eventually exceeding the critical carrier density required to excite SPP [$\mathrm{Re}(\varepsilon) < -1$]. The SPP then imprint the *LSFL-I* characteristics seeded by the second laser pulse, which is reinforced by multiple irradiations ($N_{\mathrm{DPS}} = 10$).

On the intrinsically plasmonically active metal titanium (at 800 nm wavelength) essentially the same behavior as for silicon is observed [see Fig. 7(g)–(i)], i.e. the *LSFL-I* characteristics are dominated by the second laser pulse and can be explained by a similar plasmonic effect [41]. Remarkably, also the *HSFL-II* formed in the periphery of the irradiated spots rotate, when crossing the zero delay [see the insets of Fig. 7(g) and (i)]. This further supports *hypothesis I* that the origin of *HSFL-II* lies in the early stage of energy deposition to the material.

For a better understanding of the "coherent superposition phenomenon" observed close to zero-delay, an additional set of experiments was performed at the same total peak fluence of $\phi_{0,\mathrm{tot}} = 0.2$ J/cm^2, while changing the pulse energy ratio within the sequence. Fig. 8 presents SEM micrographs of a titanium surface after irradiation with $N_{\mathrm{DPS}} = 50$ cross-polarized double-fs-pulses of three different pulse energy ratios of 60:40, 50:50, and 40:60. For a ratio of 60:40, the stronger pulse is horizontally polarized and the resulting LSFL are formed at an angle of ∼18° with respect to the vertical direction, see the yellow line in Fig. 8(a). When both pulses carry the same energy (50:50), the LSFL appear under ∼40° to the vertical [see Fig. 8(b)]. For an energy ratio of 40:60, the stronger pulse is

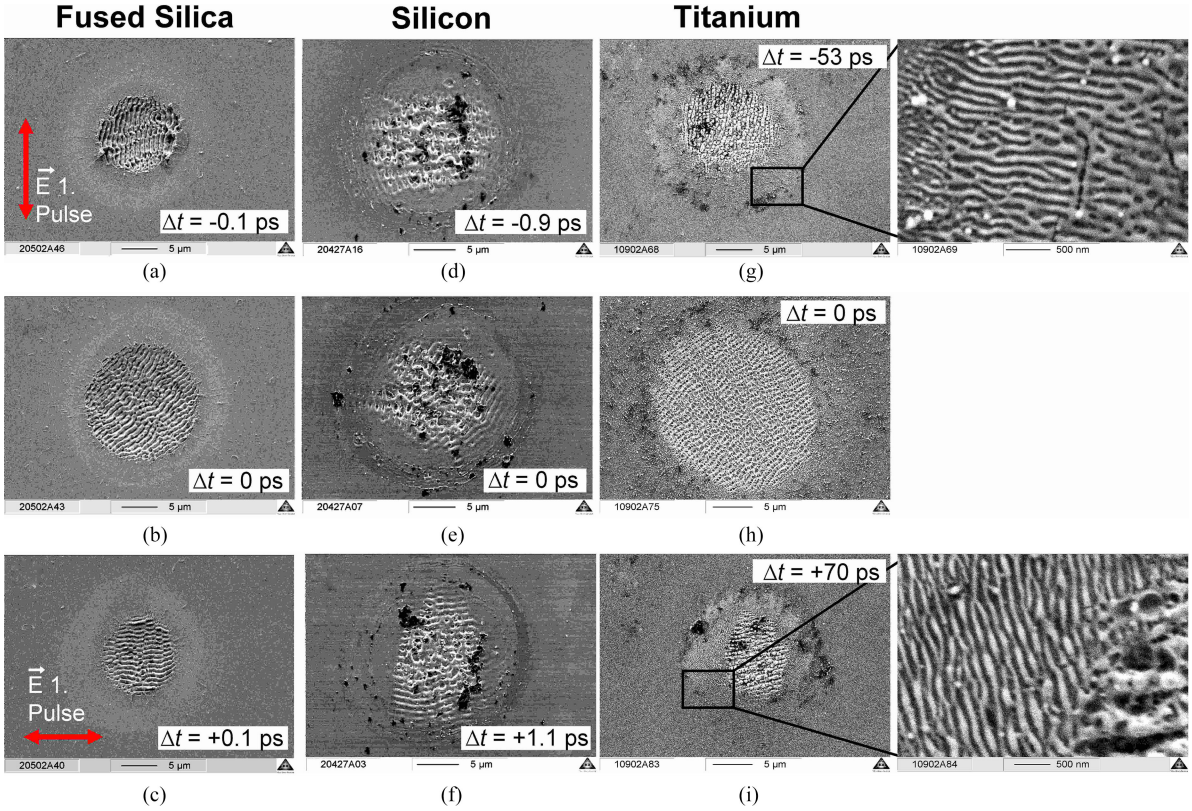

Fig. 7. Scanning electron micrographs of three different material classes upon equal energy double-fs-pulse irradiation [(a)–(c) fused silica, (d)–(f) silicon, (g)–(i) titanium] for varying inter-pulse delays between -53 ps $\leq \Delta t \leq +70$ ps. The red arrows in (a) and (c) indicate the orientation of the laser beam polarization of the first pulse arriving to the sample surface. The fused silica sample (a)–(c) was irradiated with $N_{\mathrm{DPS}} = 5$ double-pulse sequences at a total peak fluence of $\phi_{0,\mathrm{tot}} = 5.9$ J/cm^2, the silicon sample (d)–(f) was irradiated with $N_{\mathrm{DPS}} = 10$ double-pulse sequences at a total peak fluence of $\phi_{0,\mathrm{tot}} = 0.55$ J/cm^2, and the titanium sample (g)–(i) was irradiated with $N_{\mathrm{DPS}} = 50$ double-pulse sequences at a total peak fluence of $\phi_{0,\mathrm{tot}} = 0.2$ J/cm^2 [50 fs, 800 nm, 250 Hz].

vertically polarized, resulting in LSFL being tilted at an angle of $\sim$70° to the vertical direction [see Fig. 8(c)]. This experiment clearly suggests that the direction of the LIPSS can be controlled via the laser pulse energy ratio in the double-pulse sequences. These results are in line with recent results by Hashida *et al.* reporting the same effect under very similar experimental conditions [96].

Apart from the influence of the double-pulse characteristics (delay, polarization, energy ratio) on the final direction of the LIPSS, also the impact on the LIPSS period [43], [94], [97]–[101] and the LIPSS-covered spot area [39], [92], [95], [98], [101] were studied. While for semiconductors and metals the LSFL period does not significantly depend on the delay $(\Lambda_{\mathrm{LSFL}} \sim \lambda)$ [41], [94], [98], [100] , for dielectrics a transition between a metallic behavior $[\Lambda_{\mathrm{LSFL}} \sim \lambda\,(\Delta t \sim 0)]$ and a dielectric behavior $[\Lambda_{\mathrm{LSFL}} \sim \lambda/n\,(\Delta t > 1\,\mathrm{ps})]$ was reported [97], [102]. For sub-threshold conditions, the LSFL-covered surface area shows a monotonous decrease with the delay Δt, often following a mono- or bi-exponential reduction with characteristic decay times between $\sim$0.1 ps and $\sim$10 ps, depending on the material [92]. Recently, these single-color studies have been extended to a two-color scheme using parallel or cross-polarized ultrashort double-pulse sequences. The corresponding experiments for dielectrics [93], [103]–[105], semiconductors [106] and metals [41], [93], [107], [108] provided additional evidence that the LIPSS characteristics are predominantly seeded during the early stages of deposition of the optical pulse energy to the solids.

C. Time-Resolved Diffraction on LIPSS

Further support of *hypothesis I* was provided by transillumination ultrafast pump-probe experiments in the optical spectral range, studying the dynamics of the *LSFL-II* formation on fused silica by recording the first order fs-time-resolved diffraction in the 0.1 ps to 1 ns range [71], see Fig. 9.

For the first few fs-laser (pump) pulses, even before a permanent surface relief of LSFL was observed, a transient diffraction at the LSFL spatial frequencies develops within less than $\sim$300 fs, lasting for up to 1 ns (Fig. 9, upper graph: $N_{\mathrm{Pump}} = 1 - 3$). The diffraction was attributed to the formation of a transient refractive index grating (in the probe-beam transparency regime of the material), caused by the spatially modulated generation of electrons in the CB of the solid and subsequent relaxation processes [71]. The observed time scales are consistent with that for STE formation, thermal processes (heating via electron-phonon coupling and heat diffusion), and plasma relaxation.

For more than three pump pulses a permanent *LSFL-II* surface relief was observed. Hence, at $N_{\mathrm{Pump}} \geq 5$, a diffraction signal

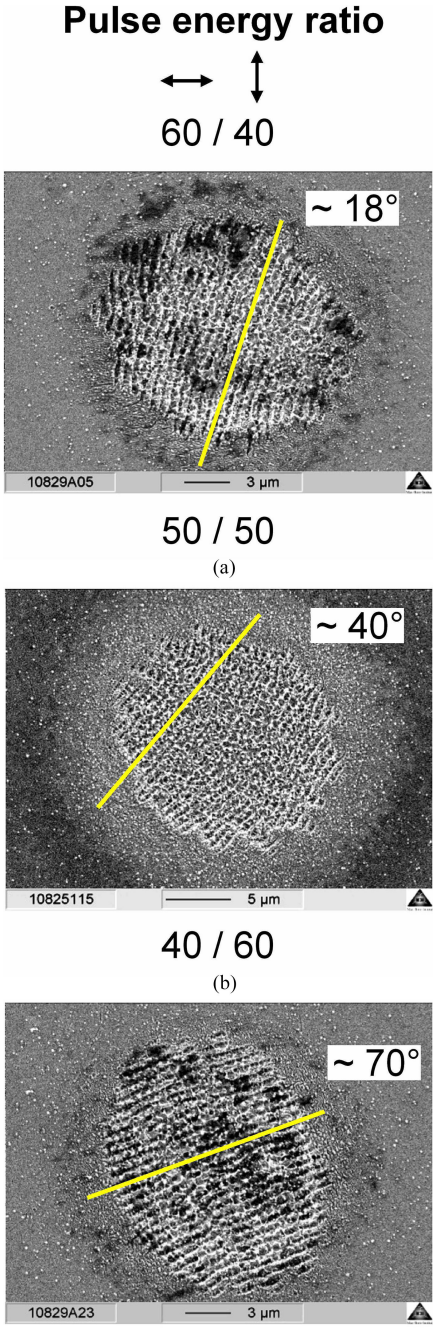

Fig. 8. Scanning electron micrographs of a titanium surface upon cross-polarized double-fs-pulse irradiation of varying pulse energy ratios [(a) 60/40: $\phi_0(\leftrightarrow) = 0.12$ J/cm^2 and $\phi_0(\updownarrow) = 0.08$ J/cm^2, (b) 50/50: $\phi_0(\leftrightarrow) = 0.1$ J/cm^2 and $\phi_0(\updownarrow) = 0.1$ J/cm^2, (c) 40/60: $\phi_0(\leftrightarrow) = 0.08$ J/cm^2 and $\phi_0(\updownarrow) = 0.12$ J/cm^2]. $N_{\mathrm{DPS}} = 50$. Δt was chosen close to zero-delay [50 fs, 800 nm, 250 Hz].

was already detected when the probe pulse arrives prior to the pump pulse. In contrast, if the probe pulse arrived after the pump pulse, the diffraction signal was almost completely screened by the optically absorbing free electron plasma generated by the pump pulse. (Fig. 9, lower graph: $N_{\mathrm{Pump}} = 5 - 20$). Hence the (delay) lapse with a reduced diffraction signal reflects the electron dynamics during the fs-laser-excitation of fused silica

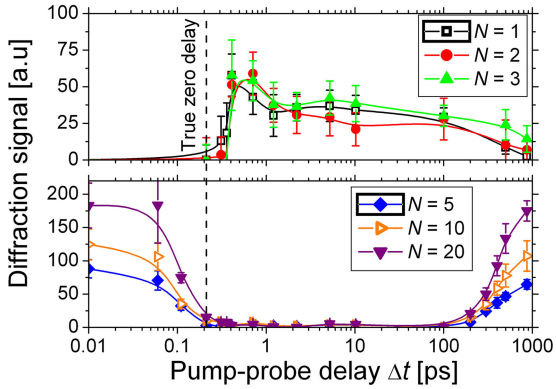

Fig. 9. First order diffraction signal [probe beam: $\lambda_{\mathrm{Probe}} = 400$ nm, $\tau_{\mathrm{Probe}} \sim 50$ fs, $\theta_{\mathrm{Probe}} = 15°$] of *LSFL-II* in fused silica measured in transmission as a function of the fs-pump-probe delay Δt upon irradiation at $\phi_0 = 3.9$ J/cm^2 by six different numbers of pump pulses $N = 1, 2, 3, 5, 10, 20$, [pump beam: $\lambda_{\mathrm{Pump}} = 800$ nm, $\tau_{\mathrm{Pump}} = 50$ fs, $\theta_{\mathrm{Pump}} = 0°$]. Note the logarithmic delay axis and the delay offset of 0.2 ps. Figure adapted from [71].

[109]. It is not directly related to the *LSFL-II* surface relief formation here.

Very recently, several groups started to perform fs-time resolved microscopy for directly imaging the temporal evolution of LIPSS [110]–[113]—a challenging task since even the larger LSFL exhibit periods that are close to the resolution limit of optical microscopy. For non-transparent materials (semiconductors and metals) this task is additionally complicated by the laser-induced ablation plasma. The latter evolves at the surface irradiated by the pump pulse for times larger than a few tens of picoseconds and screens the imaging probe pulse similar to the case depicted in the lower part of Fig. 9. According to these studies, the time required for the appearance of the first surface ridges accounts to ∼50 ps, in line with the temporal dynamics of fs-laser induced ablation at fluences close to the ablation threshold [114], [115].

V. Applications of LIPSS

The nanostructuring of different materials with LIPSS goes in hand with a change in surface characteristics. This gives rise to several applications of LIPSS covered surfaces. Here, controlled colorization due to diffraction at the LIPSS, hydrophobic/-philic behavior in wetting tests, effects of LIPSS on cell and bacterial film growth as well as the reduction of friction and wear in tribological applications will be discussed.

Most of these applications require the homogeneous processing of LIPSS on large surface areas. This is typically realized by a meandering, linewise scanning of the focused laser beam across the sample surface. The available laser technology already provides energetic ultrashort laser pulses at multi-MHz pulse repetition rates. To avoid troublesome heat-accumulation effects, sufficiently fast scanner technologies are currently developed and explored for the generation of micro-and nano-surface-textures in industrial applications [116]. In the latter reference, the surface processing of LIPSS on steel surfaces was demonstrated at scan speeds between 25 m/s and 90 m/s, employing a 2 MHz fs-laser along with a polygon scanner head.

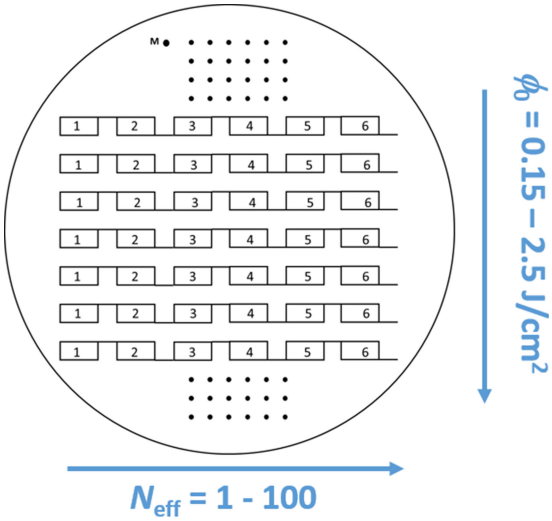

(a)

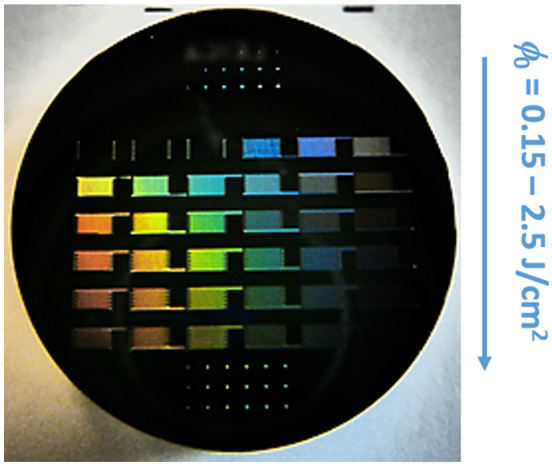

(b)

Fig. 10. (a) Scheme for laser processing. (b) Photograph of a 100Cr6 steel sample (Ø = 24 mm) after spot, line and area fs-laser processing [30 fs, 800 nm, 1 kHz]. The colors arise from optical diffraction of ambient light at laser-generated LSFL.

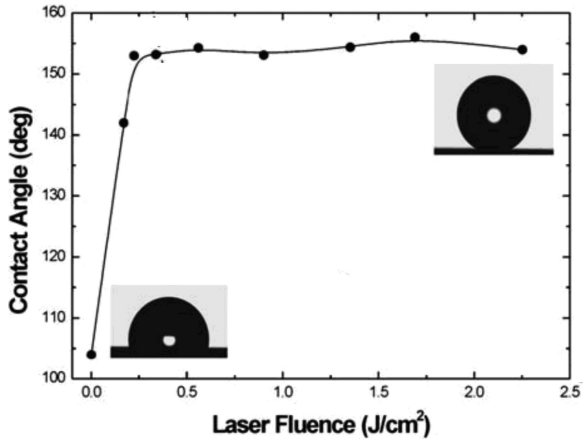

Fig. 11. Static contact angle measurements of a water drop on structured silicon surfaces plotted as a function of the laser fluence. Insets: side-view images of the droplet on the flat as well as on the structured silicon surface [127]. *Applied Physics A*, Tailoring the wetting response of silicon surfaces via fs laser structuring, Vol. 93, 2008, 819–825, V. Zorba *et al.*, (© Springer-Verlag 2008) With permission of Springer.

A. Structural Color

A promising application of LIPSS arises from the fact that they act as diffractive gratings, generating structural color. Depending on size and orientation of the ripples as well as angles of incident light and observation, different shades of colors throughout the visible part of the spectrum are feasible—compare Fig. 10(b). The period Λ of the LIPSS can be controlled by the laser wavelength, fluence and the scan speed, i.e., the number of effective pulses per spot diameter N_{eff} (for the definition see [117]), see Fig. 10(a).

The first ones to use a fs-laser to modify the optical properties of metals (aluminium, gold and platinum) were Vorobyev and Guo in 2008 [118]. Other examples for LIPSS induced structural color on different types of steel [119]–[122], copper [123], [124] and other metals and semiconductors [125] followed. For example, Dusser *et al.* systematically investigated the influence of critical laser parameters such as pulse energy, light polarization, spot size on the sample and overlapping of spots on the sample on the resulting ripples and their optical properties. With this colorimetric calibration in hand, pre-defined pictures could be reproduced using nanostructures with a user defined orientation associated with laser polarization [119]. Additionally, the spatial period of the ripples and, in turn, the color of the laser processed metal, can also be tuned by the laser wavelength. A theoretical as well as experimental study on the influence of laser wavelength on color marking on stainless steel was presented by Li *et al.* [122]. The control of color by LIPSS renders various applications viable, such as laser marking, optical data storage, anti-counterfeiting, encryption, decoration or color displays [119], [121]. In contrast to classical methods, it is extremely difficult to copy the laser generated structural color, more information can be included on smaller space and the reading procedure is straightforward, which is highly advantageous for the above listed applications [119].

B. Wetting

Next to the optical appearance, also the wetting properties of LIPSS covered surfaces change compared to non-structured materials. For instance, superhydrophobic surfaces were reported upon fs laser irradiation of silicon wafers and subsequent coating with chloroalkylsilane [126], [127]. The contact angle (CA) could be increased from 104° for the unprocessed surface up to 156°, if the peak fluence for laser processing was chosen high enough—compare Fig. 11 [127]. Due to the increased surface roughness of the LIPSS covered samples, air remains trapped underneath the liquid and thus the surface becomes superhydrophobic. Kietzig *et al.* established the fact that metallic surfaces (steel, pure metals and alloys) with initial CAs between 60° and 85° change their CA with time from superhydrophilic (CA $<$ 30°) shortly after laser processing to superhydrophobic (CA = 120°—160°), due to surface chemistry [128], [129]. Those findings were also corroborated by other groups [130]. However, the storage environment plays a decisive role for the change of surface wetting properties [129], [131].

C. Cell Growth

LIPSS covered surfaces are also of interest for medical applications. For instance, on titanium based materials, which are frequently used for joint replacements, cell adhesion was reduced, while osteointegration was enhanced and, in turn, integration and life span of the implants was increased [132]–[134]. Furthermore, it was demonstrated that cells align along the LIPSS on titanium based materials [135] and a correlation between LIPSS size and cell spreading was found [131]. On other metals, such as steel, it was shown that on the LIPSS covered surfaces adhesion behavior depends on the shape of the bacteria employed [136].

Also on semiconducting materials, such as silicon, the influence of periodic surface structures on cell colonization was studied. Here, initially no difference was observed between processed and unprocessed areas for different cell types. After 1-2 days the cells accumulated on the unstructured silicon surface [137]. In another example, polymer foils were laser structured and investigated with respect to proliferation, adhesion and orientation of mammalian cells. On polystyrene (PS) covered with LIPSS cell adhesion and proliferation was enhanced due to surface chemical changes. At LIPSS periodicities above a critical, cell type specific value the cells aligned along the nanostructures. Fig. 12 shows Chinese hamster ovary (CHO-K1) cells that are aligned along LIPSS on PS [138].

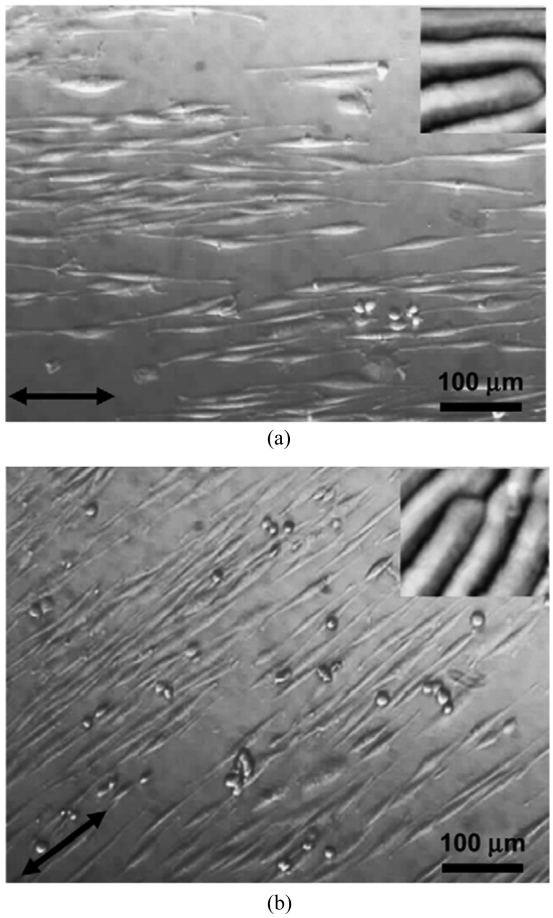

Fig. 12. Phase contrast microscopic images of CHO-K1 cells (a) 27 h and (b) 52 h after seeding on PS foils irradiated at an angle of incidence of 45°. Arrows indicate the direction of the ripples. In the insets typical magnified AFM images (1.4 μm $\times$ 1.4 μm) of the PS foils are shown [138]. Reprinted from *Biomaterials*, Vol. 29, E. Rebollar *et al*., Proliferation of aligned mammalian cells on laser-nanostructured polystyrene, 1796–1806, Copyright (2008), with permission from Elsevier.

D. Tribology

The first ones to recognize the potential of LIPSS for tribological applications were Yu and Lu in 1999 [139]. They reported improved tribological performance on micrometer sized ripples on NiP when compared to unstructured NiP surface [139]. In the following years, LIPSS on various materials, for instance carbon materials [140]–[143], nitrides [143], silicon [144], steel [145]–[152] and titanium based materials [149], [150], [153] were tested with respect to friction and wear. When comparing the tribological performance of LIPSS with periods in the range of 500-600 nm on different steel samples (100Cr6 and X30CrMoN15-1) with those on titanium based samples (pure titanium and Ti alloy Ti6Al4V) a significantly different behavior becomes evident. Under identical processing conditions, namely exciting with a linearly polarized laser (τ = 30 fs duration, λ = 790 nm center wavelength, ν = 1 kHz pulse repetition frequency, Gaussian-like beam profile with a radius $w_0\,(1/\mathrm{e}^2) \sim 140\,\mu$m with a laser peak fluence of $\phi_0 \sim 0.11\,\mathrm{J/cm}^2$ and an effective number of pulses per spot diameter of $N_{\mathrm{eff}} \sim 56$ in scan direction) ripples of periodicities of $\Lambda_{\mathrm{LSFL}} \sim 515\,\mathrm{nm}$ (Ti and X30CrMoN15-1) [150] and $\Lambda_{\mathrm{LSFL}} \sim 610\,\mathrm{nm}$ (Ti6Al4V and 100Cr6) were generated [149]. Reciprocating sliding tribological tests (RSTT) against a polished 100Cr6 steel ball ($\varnothing = 10$ mm) were performed at a normal force of $F_{\mathrm{N}} = 1.0$ N with 1000 cycles at a frequency of 1 Hz using paraffin oil or engine oil (Castrol VP-1) as lubricants—compare Fig. 13(a).

While in paraffin oil no beneficial effect on the coefficient of friction (COF) was observed in any of the tested materials, in the additivated engine oil the COF is more than a factor of two smaller on LIPSS covered Ti and Ti6Al4V compared to the non-structured surface—Fig. 13(b) [149], [150]. In line with those findings, the wear tracks on the LIPSS covered surface are notably smaller—Fig. 13(c) and (d)—and SEM—Fig. 13(e)—reveals that the LIPSS are still present after RSTT [149]. On both of the tested steel types no significant improvement was observed [149], [150].

Different aspects were taken into consideration in order to explain the observations. On one hand, the additives contained in the engine oil, in contrast to paraffin oil, seem to efficiently cover the laser structured surface and build up a gliding intermediate layer, protecting the two metals from direct contact. On the other hand, laser-induced oxidation seems to contribute to the improved tribological behavior on LIPSS covered surfaces. In contrast to titanium based materials, the improvement is less pronounced on steel, since it is of similar hardness than the counterbody [149], 150]. Additionally, the LIPSS modulation depth must be taken into account. If it is smaller than the sample-ball deformation no beneficial effect was observed in RSTT

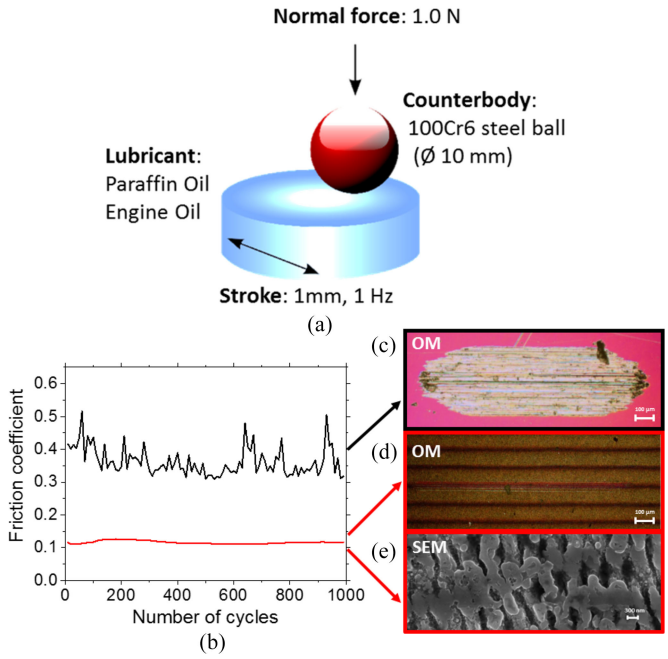

Fig. 13. Scheme for the reciprocating sliding tribological tests (a). COF versus number of cycles on the fs-LIPSS (red) and on un-structured Ti6Al4V (black) in engine oil (b). Optical micrographs (c) and (d) (OM) and high resolution scanning electron micrographs (e) (SEM) of the corresponding wear tracks taken after the tribological experiment. Figure adapted from [149].

[153]. For this reason, the shallow HSFL on titanium cannot provide the same tribological benefit as the LSFL [153].

E. Other Applications

Apart from the previously summarized applications, additional utilizations of LIPSS for surface functionalization were proposed. Several authors demonstrated the beneficial effect of LIPSS in analytical applications based on *Surface Enhanced Raman Scattering* (SERS) [154]–[157], where plasmonic excitation and field enhancement effects in the vicinity of rough surface features can enhance the spectroscopic signal by up to three orders of magnitude [155]. The LIPSS were either directly processed on bulk silver and copper surfaces [154], [157] or generated on dielectric materials and subsequently overcoated with metallic gold or silver films [155], [156].

Vorobyev *et al.* processed LIPSS directly on a tungsten incandescent lamp filament. The authors reported a local brightening of the filament and an enhanced thermal radiation emission efficiency [158]–[160]. Volkov *et al.* reported an increased X-ray emission from a LIPSS-covered metal surface for fs-laser irradiation at high intensities [161].

Romoli *et al.* investigated the application of LIPSS at the inner walls of gasoline direct injection nozzles, demonstrating improvements in the fuel atomization via a reduction of the average droplet size by $\sim$10% compared to conventional laser trepanned nozzle holes [162].

Knüttel *et al.* studied LIPSS for laser texturing in thin-film silicon photovoltaics [163]. The authors processed the structures on front contact aluminum-doped zinc oxide films by ps-laser radiation and demonstrated their suitable optical scattering capabilities.

VI. Conclusion

The current state in the field of LIPSS was reviewed. Special emphasis was placed on the question whether the LIPSS are seeded via ultrafast energy deposition mechanisms acting during the absorption of optical radiation or via self-organization after the irradiation process. Scattering, diffraction and double-pulse experiments evidenced that the ultrafast excitation stage is essential for the formation of LIPSS upon ultrashort pulse laser irradiation. Emerging technological applications of LIPSS in the fields of optics, fluidics, medicine, and tribology were outlined.

Acknowledgment

The authors would like to thank S. Binkowski (BAM 6.3), M. Lagleder, and O. Netzband (both BAM 6.7), for polishing of the metal samples, R. Koter (BAM 6.4) for help with the fs-laser system, S. Pentzien (BAM 6.4) for help with the sample characterization, S. Benemann (BAM 6.1) and M. Tischer (MBI) for SEM characterizations, and D. Spaltmann, M. Hartelt, and N. Slachciak (all BAM 6.3) for their help with the tribological tests.

References

[1] H. M. van Driel, J. E. Sipe, and J. F. Young, "Laser-induced periodic surface structure on solids: A universal phenomenon," *Phys. Rev. Lett.*, vol. 49, pp. 1955–1958, 1982.

[2] J. Bonse, J. Krüger, S. Höhm, and A. Rosenfeld, "Femtosecond laser-induced periodic surface structures," *J. Laser Appl.*, vol. 24, p. 042006, 2012.

[3] R. J. Nemanich, D. K. Biegelsen, and W. G. Hawkins, "Aligned, coexisting liquid and solid regions in laser-annealed Si," *Phys. Rev. B*, vol. 27, pp. 7817–7819, 1983.

[4] J. Bonse, S. Baudach, J. Krüger, W. Kautek, and M. Lenzner, "Femtosecond laser ablation of silicon–modification thresholds and morphology," *Appl. Phys. A*, vol. 74, pp. 19–25, 2002.

[5] S. A. Akhmanov, V. I. Emel'yanov, N. I. Koroteev, and V. N. Seminogov, "Interaction of powerful laser radiation with the surfaces of semiconductors and metals: Nonlinear optical effects and nonlinear optical diagnostics," *Sov. Phys. Usp.*, vol. 28, pp. 1084–1124, 1985.

[6] A. E. Siegman and P. M. Fauchet, "Stimulated Wood's anomalies on laser-illuminated surfaces," *IEEE J. Quantum Electron.*, vol. 22, no. 8, pp. 1384–1403, Aug. 1986.

[7] T.-H. Her, "Femtosecond-laser-induced periodic self-organized nanostructures," in *Comprehensive Nanoscience and Technology: Nanofabrication and Devices*. vol. 4, D. Andrews, G. Scholes, and G. Wiederrecht, Eds. New York, NY, USA: Academic, 2011, pp. 277–314.

[8] A. Y. Vorobyev and C. Guo, "Direct femtosecond laser surface nano/microstructuring and its applications," *Laser Photon. Rev.*, vol. 7, pp. 1–23, 2012.

[9] R. Buividas, M. Mikutis, and S. Juodkazis, "Surface and bulk structuring of materials by ripples with long and short laser pulses: Recent advances," *Prog. Quantum Electron.*, vol. 38, pp. 119–156, 2014.

[10] F. Müller, C. Kunz, and S. Gräf, "Bio-inspired functional surfaces based on laser-induced periodic surface structures," *Materials*, vol. 9, p. 476, 2016.

[11] M. Birnbaum, "Semiconductor surface damage produced by ruby lasers," *J. Appl. Phys.*, vol. 36, pp. 3688–3689, 1965.

[12] D. C. Emmony, R. P. Howson, and L. J. Willis, "Laser mirror damage in germanium at 10.6 μm," *Appl. Phys. Lett.*, vol. 23, pp. 598–600, 1973.

[13] F. Keilmann and Y. H. Bai, "Periodic surface structures frozen into CO_2 laser-melted quartz," *Appl. Phys. A*, vol. 29, pp. 9–18, 1982.

[14] J. E. Sipe, J. F. Young, J. S. Preston, and H. M. van Driel, "Laser-induced periodic surface structure. I. Theory," *Phys. Rev. B*, vol. 27, pp. 1141–1154, 1983.

[15] Z. Guosheng, P. M. Fauchet, and A. E. Siegman, "Growth of spontaneous periodic surface structures on solids during laser illumination," *Phys. Rev. B*, vol. 26, pp. 5366–5381, 1982.

[16] J. F. Young, J. S. Preston, H. M. van Driel, and J. E. Sipe, "Laser-induced periodic surface structure. II. Experiments on Ge, Si, Al, and brass," *Phys. Rev. B*, vol. 27, pp. 1155–1172, 1983.

[17] J. F. Young, J. E. Sipe, and H. M. van Driel, "Laser-induced periodic surface structure. III. Fluence regimes, the role of feedback, and details of the induced topography in germanium," *Phys. Rev. B*, vol. 30, pp. 2001–2015, 1984.

[18] J. Bonse, M. Munz, and H. Sturm, "Structure formation on the surface of indium phosphide irradiated by femtosecond laser pulses," *J. Appl. Phys.*, vol. 97, p. 013538, 2005.

[19] J. Bonse, S. Höhm, A. Rosenfeld, and J. Krüger, "Sub-100-nm laser-induced periodic surface structures upon irradiation of titanium by ti:Sapphire femtosecond laser pulses in air," *Appl. Phys. A*, vol. 110, pp. 547–551, 2013.

[20] C. Dorronsoro, J. Bonse, and J. Siegel, "Self-assembly of a new type of periodic surface structure in a copolymer by excimer laser irradiation above the ablation threshold," *J. Appl. Phys.*, vol. 114, p. 153105, 2013.

[21] J. Bonse, H. Sturm, D. Schmidt, and W. Kautek, "Chemical, morphological and accumulation phenomena in ultrashort-pulse laser ablation of TiN in air," *Appl. Phys. A*, vol. 71, pp. 657–665, 2000.

[22] A. M. Ozkan *et al.*, "Femtosecond laser-induced periodic structure writing on diamond crystals and microclusters," *Appl. Phys. Lett.*, vol. 75, pp. 3716–3718, 1999.

[23] J. Reif, F. Costache, M. Henyk, and S. V. Pandelov, "Ripples revisited: Non-classical morphology at the bottom of femtosecond laser ablation craters in transparent dielectrics," *Appl. Surf. Sci.*, vols. 197/198, pp. 891–895, 2002.

[24] Q. Wu *et al.*, "Femtosecond laser-induced periodic surface structure on diamond film," *Appl. Phys. Lett.*, vol. 82, pp. 1703–1705, 2003.

[25] A. Borowiec and H. K. Haugen, "Subwavelength ripple formation on the surfaces of compound semiconductors irradiated with femtosecond laser pulses," *Appl. Phys. Lett.*, vol. 82, pp. 4462–4464, 2003.

[26] J. Reif, O. Varlamova, S. Varlamov, and M. Bestehorn, "The role of asymmetric excitation in self-organized nanostructure formation upon femtosecond laser ablation," *Appl. Phys. A*, vol. 104, pp. 969–973, 2011.

[27] D. Dufft, A. Rosenfeld, S. K. Das, R. Grunwald, and J. Bonse, "Femtosecond laser-induced periodic surface structures revisited: A comparative study on ZnO," *J. Appl. Phys.*, vol. 105, p. 034908, 2009.

[28] J. Bonse, A. Rosenfeld, and J. Krüger, "On the role of surface plasmon polaritons in the formation of laser-induced periodic surface structures upon irradiation of silicon by femtosecond-laser pulses," *J. Appl. Phys.*, vol. 106, p. 104910, 2009.

[29] K. Sokolowski-Tinten *et al.*, "Short-pulse laser induced transient structure formation and ablation studied with time-resolved coherent XUV-scattering," *AIP Conf. Proc.*, vol. 1278, pp. 373–379, 2010.

[30] J. Z. P. Skolski *et al.*, "Laser-induced periodic surface structures: Fingerprints of light localization," *Phys. Rev. B*, vol. 85, p. 075320, 2012.

[31] J. Z. P. Skolski, G. R. B. E. Römer, J. Vincenc Obona, and A. J. Huis in't Veld, "Modeling laser-induced periodic surface structures: Finite-difference time-domain feedback simulations," *J. Appl. Phys.*, vol. 115, p. 103102, 2014.

[32] H. Zhang *et al.*, "Coherence in ultrafast laser-induced periodic surface structures," *Phys. Rev. B*, vol. 92, p. 174109, 2015.

[33] M. Huang, F. Zhao, Y. Cheng, N. Xu, and Z. Xu, "Origin of laser-induced near-subwavelength ripples: Interference between surface plasmons and incident laser," *ACS Nano*, vol. 3, pp. 4062–4070, 2009.

[34] M. Huang, Y. Cheng, F. Zhao, and Z. Xu, "The significant role of plasmonic effects in femtosecond laser-induced grating fabrication on the nanoscale," *Ann. Phys., Berlin*, vol. 525, pp. 74–86, 2013.

[35] M. Terakawa *et al.*, "Enhanced localized near field and scattered far field for surface nanophotonics applications," *Prog. Quantum Electron.*, vol. 36, pp. 194–271, 2012.

[36] G. Miyaji and K. Miyazaki, "Origin of periodicity in nanostructuring on thin film surfaces ablated with femtosecond laser pulses," *Opt. Express*, vol. 16, pp. 16265–16271, 2008.

[37] F. Garrelie *et al.*, "Evidence of surface plasmon resonance in ultrafast laser-induced ripples," *Opt. Express*, vol. 19, pp. 9035–9043, 2011.

[38] T. J.-Y. Derrien, T. E. Itina, R. Torres, T. Sarnet, and M. Sentis, "Possible surface plasmon polariton excitation under femtosecond laser irradiation of silicon," *J. Appl. Phys.*, vol. 114, p. 083104, 2013.

[39] T. J.-Y. Derrien *et al.*, "Rippled area formed by surface plasmon polaritons upon femtosecond laser double-pulse irradiation of silicon," *Opt. Express*, vol. 21, pp. 29643–29655, 2013.

[40] H. Raether, *Surface Plasmons on Smooth and Rough Surfaces and on Gratings*. Berlin, Germany: Springer-Verlag, 1988.

[41] S. Höhm, A. Rosenfeld, J. Krüger, and J. Bonse, "Laser-induced periodic surface structures on titanium upon single- and two-color femtosecond double-pulse irradiation," *Opt. Express*, vol. 23, pp. 25959–25971, 2015.

[42] W. L. Barnes, A. Dereux, and T. W. Ebbesen, "Surface plasmon subwavelength optics," *Nature*, vol. 424, pp. 824–830, 2003.

[43] S. Höhm, A. Rosenfeld, J. Krüger, and J. Bonse, "Femtosecond laser-induced periodic surface structures on silica," *J. Appl. Phys.*, vol. 112, p. 014901, 2012.

[44] P. A. Temple and M. J. Soileau, "Polarization charge model for laser-induced ripple patterns in dielectric materials," *IEEE J. Quantum Electron.*, vol. 17, no. 10, pp. 2067–2072, Oct. 1981.

[45] M. J. Soileau, "Ripple structures associated with ordered surface defects in dielectrics," *IEEE J. Quantum Electron.*, vol. 20, no. 5, pp. 464–467, May 1984.

[46] J. E. Sipe, H. M. van Driel, and J. F. Young, "Surface electrodynamics: Radiation fields, surface polaritons, and radiation remnants," *Can. J. Phys.*, vol. 63, pp. 104–113, 1985.

[47] S. Hou *et al.*, "Formation of long- and short-periodic nanoripples on stainless steel irradiated by femtosecond laser pulses," *J. Phys. D, Appl. Phys.*, vol. 44, p. 505401, 2011.

[48] J. J. Nivas *et al.*, "Direct femtosecond laser surface structuring with optical vortex beams generated by a q-plate," *Sci. Rep.*, vol. 5, 2015, Art. no. 17929.

[49] Y. Katsumata, T. Morita, Y. Morimoto, T. Shintani, and T. Saiki, "Self-organization of a periodic structure between amorphous and crystalline phases in a GeTe thin film induced by femtosecond laser pulse amorphization," *Appl. Phys. Lett.*, vol. 105, p. 031907, 2014.

[50] D. Puerto *et al.*, "Femtosecond laser-controlled self-assembly of amorphous-crystalline nanogratings in silicon," *Nanotechnology*, vol. 27, p. 265602, 2016.

[51] E. Haro-Poniatowski *et al.*, "Diffraction-assisted micropatterning of silicon surfaces by ns-laser irradiation," *J. Appl. Phys.*, vol. 115, p. 224309, 2014.

[52] D. Bäuerle, *Laser Processing and Chemistry*, 4th ed. Berlin, Germany: Springer-Verlag, 2011.

[53] V. I. Emel'yanov, "Self-organization of ordered nano- and microstructures on the semiconductor surface under the action of laser radiation," *Laser Phys.*, vol. 18, pp. 682–718, 2008.

[54] M. J. Abere, B. Torralva, and S. M. Yalisove, "Periodic surface structure bifurcation induced by ultrafast laser generated point defect diffusion in GaAs," *Appl. Phys. Lett.*, vol. 108, p. 153110, 2016.

[55] G. D. Tsibidis, E. Stratakis, and K. E. Aifantis, "Thermoplastic deformation of silicon surfaces induced by ultrashort pulsed lasers in submelting conditions," *J. Appl. Phys.*, vol. 111, p. 053502, 2012.

[56] H. M. van Driel, J. E. Sipe, and J. F. Young, "Laser-induced coherent modulation of solid and liquid surfaces," *J. Lumin.*, vol. 30, pp. 446–471, 1985.

[57] G. D. Tsibidis, M. Barberoglou, P. A. Loukakos, E. Stratakis, and C. Fotakis, "Dynamics of ripple formation on silicon surfaces by ultrashort laser pulses in subablation conditions," *Phys. Rev. B*, vol. 86, p. 115316, 2012.

[58] M. Hörstmann-Jungemann, J. Gottmann, and D. Wortmann, "Nano- and microstructuring of SiO_2 and sapphire with fs-laser induced selective etching," *J. Laser Micro Nanoeng.*, vol. 4, pp. 135–140, 2009.

[59] T. Tomita, R. Kumai, S. Matsuo, S. Hashimoto, and M. Yamaguchi, "Cross-sectional morphological profiles of ripples on Si, SiC, and HOPG," *Appl. Phys. A*, vol. 97, pp. 271–276, 2009.

[60] F. Liang, R. Vallée, and S. L. Chin, "Mechanism of nanograting formation on the surface of fused silica," *Opt. Exp.*, vol. 20, pp. 4389–4396, 2012.

[61] N. Wu *et al.*, "Nano-periodic structure formation on titanium thin film with a femtosecond laser," *J. Ceram. Soc. Jpn.*, vol. 119, pp. 898–901, 2011.

[62] X. Sedao *et al.*, "Growth twinning and generation of high-frequency surface nanostructures in ultrafast laser-induced transient melting and resolidification," *ACS Nano*, vol. 10, pp. 6995–7007, 2016.

[63] X. F. Li *et al.*, "Formation of 100-nm periodic structures on a titanium surface by exploiting the oxidation and third harmonic generation induced by femtosecond laser pulses," *Opt. Express*, vol. 22, pp. 28086–28099, 2014.

[64] S. N. Volkov, A. E. Kaplan, and K. Miyazaki, "Evanescent field at nanocorrugated dielectric surface," *Appl. Phys. Lett.*, vol. 94, p. 041104, 2009.

[65] G. A. Martsinovskiĭ *et al.*, "Ultrashort excitations of surface polaritons and waveguide modes in semiconductors," *Opt. Spectrosc.*, vol. 105, pp. 67–72, 2008.

[66] M. Straub, M. Afshar, D. Feili, H. Seidel, and K. König, "Surface plasmon polariton model of high-spatial frequency laser-induced periodic surface structure generation in silicon," *J. Appl. Phys.*, vol. 111, p. 124315, 2012.

[67] R. Buividas *et al.*, "Mechanism of fine ripple formation on surfaces of (semi)transparent materials via a half-wavelength cavity feedback," *Nanotechnology*, vol. 22, p. 055304, 2011.

[68] J. Bonse, A. Rosenfeld, and J. Krüger, "Implications of transient changes of optical and surface properties of solids during femtosecond laser pulse irradiation to the formation of laser-induced periodic surface structures," *Appl. Surf. Sci.*, vol. 257, pp. 5420–5423, 2011.

[69] E. V. Golosov *et al.*, "Near-threshold femtosecond laser fabrication of one-dimensional subwavelength nanogratings on a graphite surface," *Phys. Rev. B*, vol. 83, p. 115426, 2011.

[70] A. M. Bonch-Bruevich, M. N. Libenson, V. S. Makin, and V. V. Trubaev, "Surface electromagnetic waves in optics," *Opt. Eng.*, vol. 31, pp. 718–730, 1992.

[71] S. Höhm, A. Rosenfeld, J. Krüger, and J. Bonse, "Femtosecond diffraction dynamics of laser-induced periodic surface structures on fused silica," *Appl. Phys. Lett.*, vol. 102, p. 054102, 2013.

[72] J. S. Preston, J. E. Sipe, H. M. van Driel, and J. Luscombe, "Optical absorption in metallic-dielectric microstructures," *Phys. Rev. B*, vol. 40, pp. 3931–3941, 1989.

[73] C.-Y. Zhang *et al.*, "Colorizing silicon surface with regular nanohole arrays induced by femtosecond laser pulses," *Opt. Lett.*, vol. 37, pp. 1106–1108, 2012.

[74] P. M. Fauchet and A. E. Siegman, "Surface ripples on silicon and gallium arsenide under picosecond laser illumination," *Appl. Phys. Lett.*, vol. 40, pp. 824–826, 1982.

[75] A. Ruiz de la Cruz, R. Lahoz, J. Siegel, G. F. de la Fuente, and J. Solis, "High speed inscription of uniform, large-area laser-induced periodic surface structures in Cr films using a high repetition rate fs laser," *Opt. Lett.*, vol. 39, pp. 2491–2494, 2014.

[76] E. L. Gurevich, "Mechanisms of femtosecond LIPSS formation induced by periodic surface temperature modulation," *Appl. Surf. Sci.*, vol. 374, pp. 56–60, 2016.

[77] J. Bonse, M. Munz, and H. Sturm, "Scanning force microscopic investigations of the femtosecond laser pulse irradiation of indium phosphide in air," *IEEE Trans. Nanotechnol.*, vol. 3, no. 3, pp. 358–367, Sep. 2004.

[78] M. Huang, F. Zhao, Y. Cheng, and Z. Xu, "Effects of the amorphous layer on laser-induced subwavelength structures on carbon allotropes," *Opt. Lett.*, vol. 37, pp. 677–679, 2012.

[79] M. Couillard *et al.*, "Subsurface modifications in indium phosphide induced by single and multiple femtosecond laser pulses: A study on the formation of periodic ripples," *J. Appl. Phys.*, vol. 101, p. 033519, 2007.

[80] T. J.-Y. Derrien *et al.*, "Plasmonic formation mechanism of periodic 100-nm-structures upon femtosecond laser irradiation of silicon in water," *J. Appl. Phys.*, vol. 116, p. 074902, 2014.

[81] B. Öktem *et al.*, "Nonlinear laser lithography for indefinitely large-area nanostructuring with femtosecond pulses," *Nature Photon.*, vol. 7, pp. 897–901, 2013.

[82] T. Q. Jia *et al.*, "Alignment of nanoparticles formed on the surface of 6H-SiC crystals irradiated by two collinear femtosecond laser beams," *Appl. Phys. Lett.*, vol. 88, p. 111117, 2006.

[83] R. Le Harzic, D. Dörr, D. Sauer, F. Stracke, and H. Zimmermann, "Generation of high spatial frequency ripples on silicon under ultrashort laser pulses irradiation," *Appl. Phys. Lett.*, vol. 98, p. 211905, 2011.

[84] G. Li *et al.*, "Evolution of titanium surfaces irradiated by femtosecond laser pulses with different wavelengths," *Proc. SPIE*, vol. 8769, p. 87691V, 2013.

[85] P. Nürnberger *et al.*, "Influence of substrate microcrystallinity on the orientation of laser-induced periodic surface structures," *J. Appl. Phys.*, vol. 118, p. 134306, 2015.

[86] K. Okamuro *et al.*, "Laser fluence dependence of periodic grating structures formed on metal surfaces under femtosecond laser pulse irradiation," *Phys. Rev. B*, vol. 82, p. 165417, 2010.

[87] L. Gemini *et al.*, "Metal-like self-organization of periodic nanostructures on silicon and silicon carbide under femtosecond laser pulses," *J. Appl. Phys.*, vol. 114, no. 194903, 2013.

[88] J. Bonse and J. Krüger, "Pulse number dependence of laser-induced periodic surface structures for femtosecond laser irradiation of silicon," *J. Appl. Phys.*, vol. 108, p. 034903, 2010.

[89] C. Wang, H. Huo, M. Johnson, M. Shen, and E. Mazur, "The thresholds of surface nano-/micro-morphology modifications with femtosecond laser pulse irradiations," *Nanotechnology*, vol. 21, p. 075304, 2010.

[90] C. Albu, A. Dinescu, M. Filipescu, M. Ulmeanu, and M. Zamfirescu, "Periodical structures induced by femtosecond laser on metals in air and liquid environments," *Appl. Surf. Sci.*, vol. 278, pp. 347–351, 2013.

[91] G. Miyaji, K. Miyazaki, K. Zhang, T. Yoshifuji, and J. Fujita, "Mechanism of femtosecond-laser-induced periodic nanostructure formation on crystalline silicon surface immersed in water," *Opt. Express*, vol. 20, pp. 14848–14856, 2012.

[92] S. Höhm, A. Rosenfeld, J. Krüger, and J. Bonse, "Area dependence of femtosecond laser-induced periodic surface structures for varying band gap materials after double pulse excitation," *Appl. Surf. Sci.*, vol. 278, pp. 7–12, 2013.

[93] S. Höhm, M. Herzlieb, A. Rosenfeld, J. Krüger, and J. Bonse, "Dynamics of the formation of laser-induced periodic surface structures (LIPSS) upon femtosecond two-color double-pulse irradiation of metals, semiconductors, and dielectrics," *Appl. Surf. Sci.*, vol. 374, pp. 331–338, 2016.

[94] S. Höhm, M. Rohloff, A. Rosenfeld, J. Krüger, and J. Bonse, "Dynamics of the formation of laser-induced periodic surface structures on dielectrics and semiconductors upon femtosecond laser pulse irradiation sequences," *Appl. Phys. A*, vol. 110, pp. 553–557, 2013.

[95] T. J.-Y. Derrien *et al.*, "Rippled area formed by surface plasmon polaritons upon femtosecond laser double-pulse irradiation of silicon: The role of carrier generation and relaxation processes," *Appl. Phys. A*, vol. 117, pp. 77–81, 2014.

[96] M. Hashida *et al.*, "Orientation of periodic grating structures controlled by double-pulse irradiation," *Appl. Phys. A*, vol. 122, p. 484, 2016.

[97] M. Rohloff *et al.*, "Formation of laser-induced periodic surface structures on fused silica upon multiple cross-polarized double-femtosecond-laser-pulse irradiation sequences," *J. Appl. Phys.*, vol. 110, p. 014910, 2011.

[98] M. Barberoglou *et al.*, "The influence of ultra-fast temporal energy regulation on the morphology of Si surfaces through femtosecond double pulse laser irradiation," *Appl. Phys. A*, vol. 113, pp. 273–283, 2013.

[99] L. Gemini *et al.*, "Periodic surface structures on titanium self-organized upon double femtosecond pulse exposures," *Appl. Surf. Sci.*, vol. 336, pp. 349–353, 2015.

[100] Y. Furukawa *et al.*, "Demonstration of periodic nanostructure formation with less ablation by double-pulse laser irradiation on titanium," *Appl. Phys. Lett.*, vol. 108, p. 264101, 2016.

[101] M. Barberoglou *et al.*, "Controlling ripples' periodicity using temporally delayed femtosecond laser double pulses," *Opt. Express*, vol. 21, pp. 18501–18508, 2013.

[102] G. Du *et al.*, "Ultrafast electron dynamics manipulation of laser induced periodic ripples via a train of shaped pulses," *Laser Phys. Lett.*, vol. 10, p. 026003, 2013.

[103] S. Höhm, M. Herzlieb, A. Rosenfeld, J. Krüger, and J. Bonse, "Laser-induced periodic surface structures on fused silica upon cross-polarized two-color double-fs-pulse irradiation," *Appl. Surf. Sci.*, vol. 336, pp. 39–42, 2015.

[104] S. Guizard *et al.*, "Ultrafast breakdown of dielectrics: Energy absorption mechanisms investigated by double pulse experiments," *Appl. Surf. Sci.*, vol. 336, pp. 206–211, 2015.

[105] S. Höhm, M. Herzlieb, A. Rosenfeld, J. Krüger, and J. Bonse, "Formation of laser-induced periodic surface structures on fused silica upon two-color double-pulse irradiation," *Appl. Phys. Lett.*, vol. 103, p. 254101, 2013.

[106] S. Höhm, M. Herzlieb, A. Rosenfeld, J. Krüger, and J. Bonse, "Femtosecond laser-induced periodic surface structures on silicon upon polarization controlled two-color double-pulse irradiation," *Opt. Express*, vol. 23, pp. 61–71, 2015.

[107] M. Gedvilas, J. Mikšys, and G. Račiukaitis, "Flexible periodical micro- and nano-structuring of a stainless steel surface using dual-wavelength double-pulse picosecond laser irradiation," *RSC Adv.*, vol. 5, pp. 75075–75080, 2015.

[108] J. Cong, J. Yang, B. Zhao, and X. Xu, "Fabricating subwavelength dot-matrix surface structures of molybdenum by transient correlated actions of two-color femtosecond laser beams," *Opt. Express*, vol. 23, pp. 5357–5367, 2015.

[109] J. Siegel *et al.*, "Plasma formation and structural modification below the visible ablation threshold in fused silica upon femtosecond laser irradiation," *Appl. Phys. Lett.*, vol. 91, p. 082902, 2007.

[110] R. D. Murphy, B. Torralva, D. P. Adams, and S. M. Yalisove, "Pump-probe imaging of laser-induced periodic surface structures after ultrafast irradiation of Si," *Appl. Phys. Lett.*, vol. 103, p. 141104, 2013.

[111] X. Jia *et al.*, "Dynamics of femtosecond laser-induced periodic surface structures on silicon by high spatial and temporal resolution imaging," *J. Appl. Phys.*, vol. 115, p. 143102, 2014.

[112] K. R. Kafka *et al.*, "Time-resolved measurement of single pulse femtosecond laser-induced periodic surface structure formation induced by a pre-fabricated surface groove," *Opt. Express*, vol. 23, pp. 19432–19441, 2015.

[113] D. Puerto, M. Garcia-Lechuga, J. Solis, and J. Siegel, "Study of phase change LIPSS formation in Si by fs-resolved microscopy," presented at the Conf. Lasers Electro-Opt., San Jose, CA, USA, 2016, Paper STh1Q.1.

[114] J. Bonse, G. Bachelier, J. Siegel, and J. Solis, "Time- and space-resolved dynamics of melting, ablation, and solidification phenomena induced by femtosecond laser pulses in germanium," *Phys. Rev. B*, vol. 74, p. 134106, 2006.

[115] D. von der Linde and K. Sokolowski-Tinten, "The physical mechanisms of short-pulse laser ablation," *Appl. Surf. Sci.*, vols. 154/155, pp. 1–10, 2000.

[116] G. Mincuzzi, L. Gemini, M. Faucon, and R. Kling, "Extending ultrashort pulse laser texturing over large area," *Appl. Surf. Sci.*, vol. 386, pp. 65–71, 2016.

[117] J. Bonse, G. Mann, J. Krüger, M. Marcinkowski, and M. Eberstein, "Femtosecond laser-induced removal of silicon nitride layers from doped and textured silicon wafers used in photovoltaics," *Thin Solid Films*, vol. 542, pp. 420–425, 2013.

[118] A. Y. Vorobyev and C. Guo, "Colorizing metals with femtosecond laser pulses," *Appl. Phys. Lett.*, vol. 92, p. 041914, 2008.

[119] B. Dusser *et al.*, "Controlled nanostructures formation by ultra fast laser pulses for color marking," *Opt. Express*, vol. 18, pp. 2913–2924, 2010.

[120] M. S. Ahsan, F. Ahmed, Y. G. Kim, M. S. Lee, and M. B. G. Jun, "Colorizing stainless steel surface by femtosecond laser induced micro/nano-structures," *Appl. Surf. Sci.*, vol. 257, pp. 7771–7777, 2011.

[121] J. Yao *et al.*, "Selective appearance of several laser-induced periodic surface structure patterns on a metal surface using structural colors produced by femtosecond laser pulses," *Appl. Surf. Sci.*, vol. 258, pp. 7625–7632, 2012.

[122] G. Li *et al.*, "Femtosecond laser color marking stainless steel surface with different wavelengths," *Appl. Phys. A*, vol. 118, pp. 1189–1196, 2015.

[123] Z. Ou, M. Huang, and F. Zhao, "Colorizing pure copper surface by ultrafast laser-induced near-subwavelength ripples," *Opt. Express*, vol. 22, pp. 17254–17265, 2014.

[124] J. Long *et al.*, "Superhydrophobic and colorful copper surfaces fabricated by picosecond laser induced periodic nanostructures," *Appl. Surf. Sci.*, vol. 311, pp. 461–467, 2014.

[125] A. A. Ionin *et al.*, "Femtosecond laser color marking of metal and semiconductor surfaces," *Appl. Phys. A*, vol. 107, pp. 301–305, 2012.

[126] M. Barberoglou *et al.*, "Bio-inspired water repellent surfaces produced by ultrafast laser structuring of silicon," *Appl. Surf. Sci.*, vol. 255, pp. 5425–5429, 2009.

[127] V. Zorba *et al.*, "Tailoring the wetting response of silicon surfaces via fs laser structuring," *App. Phys. A*, vol. 93, pp. 819–825, 2008.

[128] A.-M. Kietzig *et al.*, "Laser-patterned super-hydrophobic pure metallic substrates: Cassie to Wenzel wetting transitions," *J. Adhesion Sci. Technol.*, vol. 25, pp. 2789–2809, 2011.

[129] A.-M. Kietzig, S. G. Hatzikiriakos, and P. Englezos, "Patterned superhydrophobic metallic surfaces," *Langmuir*, vol. 25, pp. 4821–4827, 2009.

[130] P. Bizi-bandoki, S. Valette, E. Audouard, and S. Benayoun, "Time dependency of the hydrophilicity and hydrophobicity of metallic alloys subjected to femtosecond laser irradiations," *Appl. Surf. Sci.*, vol. 273, pp. 399–407, 2013.

[131] O. Raimbault *et al.*, "The effects of femtosecond laser-textured Ti-6Al-4V on wettability and cell response," *Mater. Sci. Eng. C*, vol. 69, pp. 311–320, 2016.

[132] J. R. Bush, B. K. Nayak, L. S. Nair, M. C. Gupta, and C. T. Laurencin, "Improved bio-implant using ultrafast laser induced self-assembled nanotexture in titanium," *J. Biomed. Mater. Res. B*, vol. 97, pp. 299–305, 2011.

[133] A. Cunha *et al.*, "Human mesenchymal stem cell behavior on femtosecond laser-textured Ti-6Al-4V surfaces," *Nanomed., Lond.*, vol. 10, pp. 725–739, 2015.

[134] A. Cunha *et al.*, "Femtosecond laser surface texturing of titanium as a method to reduce the adhesion of staphylococcus Aureus and biofilm formation," *Appl. Surf. Sci.*, vol. 360, pp. 485–493, 2016.

[135] T. Shinonaga *et al.*, "Formation of periodic nanostructures using a femtosecond laser to control cell spreading on titanium," *Appl. Phys. B*, vol. 119, pp. 493–496, 2015.

[136] N. Epperlein *et al.*, "Influence of femtosecond laser produced nanostructures on biofilm growth on steel," *Appl. Surf. Sci.*, to be published.

[137] K. Wallat *et al.*, "Cellular reactions toward nanostructured silicon surfaces created by laser ablation," *J. Laser Appl.*, vol. 24, p. 042016, 2012.

[138] E. Rebollar *et al.*, "Proliferation of aligned mammalian cells on laser-nanostructured polystyrene," *Biomaterials*, vol. 29, pp. 1796–1806, 2008.

[139] J. J. Yu and Y. F. Lu, "Laser-induced ripple structures on Ni–P substrates," *Appl. Surf. Sci.*, vol. 148, pp. 248–252, 1999.

[140] A. Mizuno *et al.*, "Friction properties of the DLC film with periodic structures in nano-scale," *Tribol. Online*, vol. 1, pp. 44–48, 2006.

[141] N. Yasumaru, K. Miyazaki, and J. Kiuchi, "Control of tribological properties of diamond-like carbon films with femtosecond-laser-induced nanostructuring," *Appl. Surf. Sci.*, vol. 254, pp. 2364–2368, 2008.

[142] M. Pfeiffer *et al.*, "Ripple formation in various metals and super-hard tetrahedral amorphous carbon films in consequence of femtosecond laser irradiation," *Appl. Phys. A*, vol. 110, pp. 655–659, 2013.

[143] N. Yasumaru, K. Miyazaki, J. Kiuchi, and E. Sentoku, "Frictional properties of diamond-like carbon, glassy carbon and nitrides with femtosecond-laser-induced nanostructure," *Diamond Relat. Mater.*, vol. 20, pp. 542–545, 2011.

[144] J. Eichstädt, G. R. B. E. Römer, and A. J. Huis in't Veld, "Towards friction control using laser-induced periodic surface structures," *Phys. Procedia*, vol. 12, pp. 7–15, 2011.

[145] M. Duarte *et al.*, "Increasing lubricant film lifetime by grooving periodical patterns using laser interference metallurgy," *Adv. Eng. Mater.*, vol. 10, pp. 554–558, 2008.

[146] A. Rosenkranz, L. Reinert, C. Gachot, and F. Mücklich, "Alignment and wear debris effects between laser-patterned steel surfaces under dry sliding conditions," *Wear*, vol. 318, pp. 49–61, 2014.

[147] C. Gachot *et al.*, "Dry friction between laser-patterned surfaces: Role of alignment, structural wavelength and surface chemistry," *Tribol. Lett.*, vol. 49, pp. 193–202, 2013.

[148] Z. Wang, Q. Zhao, and C. Wang, "Reduction of friction of metals using laser-induced periodic surface nanostructures," *Micromachines*, vol. 6, pp. 1606–1616, 2015.

[149] J. Bonse *et al.*, "Femtosecond laser-induced periodic surface structures on steel and titanium alloy for tribological applications," *Appl. Phys. A*, vol. 117, pp. 103–110, 2014.

[150] J. Bonse *et al.*, "Tribological performance of femtosecond laser-induced periodic surface structures on titanium and a high toughness bearing steel," *Appl. Surf. Sci.*, vol. 336, pp. 21–27, 2015.

[151] J. Voyer *et al.*, "Friction reduction through sub-micro laser surface modifications," *Tribologie + Schmierungstechnik*, vol. 62, pp. 13–18, 2015.

[152] I. Gnilitskyi *et al.*, "Nano patterning of AISI 316L stainless steel with nonlinear laser lithography: Sliding under dry and oil-lubricated conditions," *Tribol. Int.*, vol. 99, pp. 67–76, 2016.

[153] J. Bonse *et al.*, "Tribological performance of sub-100-nm femtosecond laser-induced periodic surface structures on titanium," *Appl. Surf. Sci.*, vol. 374, pp. 190–196, 2016.

[154] H.-W. Chang *et al.*, "Nanostructured Ag surface fabricated by femtosecond laser for surface-enhanced Raman scattering," *J. Coll. Interface Sci.*, vol. 360, pp. 305–308, 2011.

[155] R. Buividas, P. R. Stoddart, and S. Juodkazis, "Laser fabricated ripple substrates for surface-enhanced Raman scattering," *Ann. Physik, Berlin*, vol. 524, pp. L5–L10, 2012.

[156] E. Rebollar, M. Castillejo, and T. A. Ezquerra, "Laser induced periodic surface structures on polymer films: From fundamentals to applications," *Eur. Polym. J.*, vol. 73, pp. 162–174, 2015.

[157] H. Messaoudi *et al.*, "Femtosecond-laser induced periodic surface structures for surface enhanced Raman spectroscopy of biomolecules," in *Progress in Nonlinear Nano-Optics*, S. Sakabe, C. Lienau, and R. Grunwald, Eds. Basel, Switzerland: Springer, 2014, pp. 207–219.

[158] A. Y. Vorobyev, V. S. Makin, and C. Guo, "Brighter light sources from black metal: Significant increase in emission efficiency of incandescent light sources," *Phys. Rev. Lett.*, vol. 102, p. 234301, 2009.

[159] K. C. Mishra, M. Zachau, and R. E. Levin, "Comment on 'brighter light sources from black metal: Significant increase in emission efficiency of incandescent light sources'," *Phys. Rev. Lett.*, vol. 103, p. 269401, 2009.
[160] A. Y. Vorobyev, V. S. Makin, and C. Guo, "Vorobyev, Makin, and Guo reply," *Phys. Rev. Lett.*, vol. 103, p. 269402, 2009.
[161] R. V. Volkov, D. M. Golishnikov, V. M. Gordienko, and A. B. Savel'ev, "Overheated plasma at the surface of a target with a periodic structure induced by femtosecond laser radiation," *J. Exp. Theor. Phys. Lett.*, vol. 77, pp. 473–476, 2003.
[162] L. Romoli *et al.*, "Ultrashort pulsed laser drilling and surface structuring of microholes in stainless steels," *CIRP Ann. Manuf. Technol.*, vol. 63, pp. 229–232, 2014.
[163] T. Knüttel, S. Bergfeld, and S. Haas, "Laser texturing of surfaces in thin-film silicon photovoltaics—A comparison of potential processes," *J. Laser Micro Nanoeng.*, vol. 8, pp. 222–229, 2013.

Jörn Bonse received the Diploma degree in physics from the University Hannover, Hannover, Germany, in 1996, and the Ph.D. degree in physics from the Technical University Berlin, Germany, in 2001.

He occupied various research positions at institutions, such as the Max-Born-Institute for Nonlinear Optics and Short Pulse Spectroscopy, Berlin, the Spanish National Research Council, Madrid, Spain, and the Laser Zentrum Hannover, Germany. He was appointed as a Senior Laser Application Specialist with the Newport's Spectra-Physics Lasers Division, Stahnsdorf, Germany. He is currently a Senior Scientist with the Federal Institute for Materials Research and Testing, Berlin. He has coauthored more than 100 refereed journal publications and holds two patents. His research interests include fundamentals and applications of laser–matter interaction, laser-induced micro- and nanostructures, time-resolved optical techniques, and laser processes in photovoltaics. In 2014, he was appointed as an Associated Editor for the journal *Optics Express* of the Optical Society of America (OSA).

Dr. Bonse is a member of the German Physical Society. He received the 2013 OSA Outstanding Reviewer Award, and he also received the 1999 Award for Applied Research presented by the federal German state Thuringia for the development of high-power fiber lasers.

Sandra Höhm was born in Dortmund, Germany, in 1983. She received the Dipl.-Ing. (FH) degree in applied physics from the University of Applied Sciences, Münster, Germany, in 2008, and the Ph.D. degree in experimental physics from the Technical University Berlin, Germany, in 2014. From 2008 to 2010, she was a Project Engineer Optics for a company producing high-power laser processing optics and beam delivery systems (Highyag, Stahnsdorf, Germany). From 2010 to 2015, she was a Researcher with the Max-Born-Institute for Nonlinear Optics and Short Pulse Spectroscopy, Berlin. Her research interests include laser–matter interaction, surface functionalization, and laser fabrication of nanostructured surfaces, especially laser-induced periodic surface structures.

Sabrina V. Kirner received the Diploma degree in chemistry from the Friedrich-Alexander University of Erlangen-Nuremberg, Erlangen, Germany, in 2010, and the Ph.D. degree in photophysical characterization of electron donor-acceptor systems for solar energy conversion in the research group of Prof. Dirk M. Guldi in summer 2015.

During her Ph.D. degree, she joined Prof. Shunichi Fukuzumi's Group of the Osaka University, Japan, as a Visiting Researcher. She is currently with the Federal Institute for Materials Research and Testing, Berlin, Germany. Her research focuses on fs-laser structuring of inorganic materials, including characterization and tribological behavior of the nano- and microstructured surfaces.

Arkadi Rosenfeld received the Ph.D. degree in semiconductor engineering from the Humboldt-University, Berlin, Germany, in 1976.

Between 1976 and 1992, he was a Scientific Assistant with the Central Institute for Optics and Spectroscopy, Berlin. From 1992, he was a Scientific Member in the material research group of the Max-Born-Institute (MBI) for Nonlinear Optics and Short Pulse Spectroscopy, Berlin. In 1998, he became a Scientific Project Manager of the ultrashort laser material-modification group of the MBI. In 2015, he left the MBI for retirement. He is the author of more than 90 scientific publications.

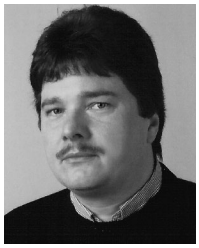

Jörg Krüger was born in 1963. He received the Diploma degree in physics from the Friedrich-Schiller-University Jena, Germany, and the doctoral degree from the Brandenburg University of Technology Cottbus, Germany.

In 1991, he joined the Federal Institute for Materials Research and Testing, Berlin, Germany, as a Research Assistant, where he is currently the acting Head of the Division 6.4 Nanomaterial Technologies. He is the (co-)author of more than 150 open literature publications. His research interests include short and ultrashort pulse laser materials processing, laser applications for the preservation of the cultural heritage, and laser safety issues.